A Neuromuscular-Model Based Control Strategy For Powered Ankle-Foot Prostheses

by

Michael Frederick Eilenberg

B.S. Computer & Systems Engineering
B.S. Mechanical Engineering
Rensselaer Polytechnic Institute, 2006

Submitted to the Department of Mechanical Engineering
in partial fulfillment of the requirements for the degree of

Master of Science in Mechanical Engineering

at the

MASSACHUSETTS INSTITUTE OF TECHNOLOGY

February 2009

Author .....
Department of Mechanical Engineering
December 19, 2008

Certified by .....
Hugh Herr
Associate Professor of Media Arts and Sciences
Assistant Professor of Health Sciences and Technology
Thesis Supervisor

Read by .....
Kamal Youcef-Toumi
Professor of Mechanical Engineering
Thesis Reader

Accepted by .....
David E. Hardt
Chairman, Department Committee on Graduate Students

A Neuromuscular-Model Based Control Strategy for Powered Ankle-Foot Prostheses

by

Michael Frederick Eilenberg

Submitted to the Department of Mechanical Engineering
on December 19, 2008, in partial fulfillment of the
requirements for the degree of
Master of Science in Mechanical Engineering

Abstract

In the development of a powered ankle-foot prosthesis, it is desirable to provide the prosthesis with the ability to exhibit human-like dynamics. A simple method for achieving this goal involves trajectory tracking, where a specific target torque trajectory is known, and the controller issues commands to follow the trajectory as closely as possible. However, without a methodology to update the desired trajectory in real time, this type of control scheme is limited in that it cannot adapt to externally-applied disturbances. Adaptation is critical in the field of prosthetics. A prosthesis must be able to adjust to variable terrain and respond to changes in behavior of the wearer. In this thesis, we hypothesize that a powered ankle-foot prosthesis that is controlled using a positive-force-feedback reflex of a Hill-type posterior leg muscle will exhibit biologically-consistent adaptive changes in stance phase behavior across terrain. To evaluate this hypothesis, a controller for a powered ankle-foot prosthesis is advanced that comprises a neuromuscular model consisting of a single, effective plantar flexor muscle with positive force feedback and an effective dorsiflexor consisting of a proportional-derivative impedance controller. Selected parameters of this hybrid controller were optimized to best match the torque-angle relationship of an intact, biological ankle from a weight and height-matched individual with intact limbs. The torque-tracking capabilities of the electromechanical system were evaluated, and a control system was developed to enable the prosthesis to produce human-like ankle mechanics. Clinical trials were performed on a healthy, bilateral amputee study participant at two separate level-ground walking speeds, as well as for ramp ascent and descent walking at self-selected speeds. The neuromuscular reflex model, when used as the basis of the prosthetic controller during these trials, produced ankle torques in qualitative agreement with values from the weight and height-matched individual with intact limbs. This agreement included an impedance modulation in the initial stance period, as well as a biologically consistent trend of increasing prosthesis net work for correspondingly increasing floor inclinations.

Thesis Supervisor: Hugh Herr
Title: Associate Professor of Media Arts and Sciences
Assistant Professor of Health Science and Technology

Acknowledgements

The work presented in this thesis would not have been possible without the support of all those around me. I would like to express my sincere thanks to the following people:

My thesis advisor, Hugh Herr, for his insightful direction and guidance over the past two years and for his genuine desire to help me succeed;

The entire Biomechatronics Group for being a great bunch of people with whom to work;

Hartmut Geyer, for always being there to answer questions about his muscle model, even from halfway around the world;

Samuel Au, for offering his valuable insight into Mechatronic system design and control;

Chris Barnhart, for all his help in taming the beast that is the ankle hardware, and teaching me so much about electronics and embedded systems;

Ernesto Martinez and Grant Elliott, for the late-night/early-morning laughs in lab, and for always being there to bounce around ideas;

Pavitra Krishnaswamy and Todd Farrell for the informative biomechanics discussions, and for actually laughing at my jokes;

Ken Endo, for his help in obtaining the biological data, and getting me started with the optimization;

Waleed Farahat, for his advice pertaining to control system design;

Bruce Deffenbaugh, for sharing his experience and providing advice on approaching tough problems;

Professor David Trumper, for his helpful academic guidance;

Professor Kamal Youcef-Toumi, for graciously offering to read my thesis;

My roommate for the past two years, Vijay Divi, for his wise-graduate-student advice, thesis tips, and of course, being a great pal;

My friends, both at MIT and elsewhere, for understanding when I would lock myself in the research-cave for extended periods of time;

Finally, I'd like to thank my parents, Heléna and Steven, and my sister, Sammy, for their incomparable love and support.

Contents

List of Figures

List of Tables

List of Terms

Dorsiflexion: A motion of the foot such that the forefoot rotates upwards towards the front of the shin.

Plantar flexion: The opposite of dorsiflexion; a motion of the foot such that the forefoot rotates away from the shin

Prosthetic Pyramid: A coupling often used in the prosthetics industry to join components together.

Sagittal Plane: The plane dividing the body into left and right sections.

1. Introduction

1.1. History of Lower-Limb Prosthesis Control

Although lower-limb prostheses have been employed for centuries, only in the past few decades have computer-controlled, active prostheses become a reality. The broader functionality provided by the sensing and actuation of these "smart" robotic prostheses over the conventional passive ones has the potential to greatly improve the lives of amputees. However, with the advent of robotic prostheses comes the challenge of controlling these devices to work in concert with their wearers.

Active prostheses can be controlled using local sensors, or external commands from the wearer such as electromyography (EMG). Today's non-invasive EMG detection requires a pair of electrodes arranged on the skin over a muscle of interest to provide an estimate of muscle activation. It is, however, difficult to obtain clear activation measurements of specific muscles due to cross-talk from adjacent muscles, noise from changes in skin conductance, mechanical artifacts, and other factors [16].

Unlike arm or hand prostheses, which require specific information from the user to determine intent, a lower limb prosthesis can also take advantage of the periodicity of the human gait cycle and utilize local sensing to predict the next likely course of action at any given time. This onboard sensing and control allows for some level of prosthesis autonomy. A multitude of computer-controlled prostheses have utilized this local sensing and control strategy. In the development of a quasi-passive prosthetic knee, researchers [8] used a combination of onboard strain gauges as input to a controller for the modulation of knee damping over the gait cycle. Similarly, during the development of a powered ankle-foot prosthesis, researchers [1] used foot-switches to determine gait state and developed a finite-state-machine based impedance controller for level-ground walking conditions. Further work involved the use of EMG signals to control the transition between level-ground and stair ambulation [2]. Such rule-based control methods, although simple to tune and easy to understand, are, without the high-level tuning strategies like those in [2], only effective for the small set of walking conditions for which they apply, and therefore have limited ability to adapt to changing terrain or amputee gait speed. Furthermore, the use of such control strategies offers little insight into human neuromechanics, since the underlying musculoskeletal biomechanics and neural reflexes of the biologic system are not modeled.

In contrast, a controller can maintain a model of a system that produces the desired behavior and issue control signals to the prosthesis based on the model state. With this type of control strategy, the control commands are emergent of the inherent structure of the model, and therefore need not follow any single target state trajectory. One possible model for use in prosthesis control is a neuromuscular architecture [5] that has been introduced to implement stretch-reflex based positive force feedback control on a Hill-type muscle model. This neuromuscular model has successfully been incorporated into a two-segment leg model to produce a hopping gait with stable stride energy. In addition, it is hypothesized that running gaits may be possible using a similar control strategy [5]. The success of this neuromuscular architecture in stabilizing a hopping gait

suggests that other repetitive tasks, such as human walking, may be well described by the model.

1.2. Thesis Objectives

The primary goal of this thesis is to evaluate a positive-force feedback reflex of a Hill-type muscle model for use in controlling a powered ankle-foot prosthesis. We hypothesize that the resulting torque profile produced by the prosthesis will be in qualitative agreement with that of a biological ankle of a healthy normal study participant at multiple walking speeds. In addition, we anticipate that this neuromuscular model will produce biologically-consistent modulation of positive net ankle work across different walking slopes. In this thesis, we evaluate these hypotheses by modeling the plantar flexor muscles in the human calf as a single, effective muscle. Select parameters of this muscle model are subsequently optimized to best match the effective muscle behavior of a normal intact human ankle. Finally, clinical trials are conducted on a healthy bi-lateral amputee study participant wearing the reflex controlled powered prosthesis. The performance of the prosthesis is then compared to the mechanics of an intact ankle from a weight and height-matched individual with intact limbs.

1.3. Chapter Summary

Chapter 2 describes the normal biomechanics of level-ground human walking as background material for the thesis.

Chapter 3 introduces the finite state machine, reflex-driven muscle model, and dorsiflexor model. Ankle behavior from biologic walking data is presented as the target joint behavior. An optimization is then presented for tuning the model parameters using this target behavior. The chapter concludes with the optimization results as compared to the biological ankle behavior.

In Chapter 4, the prosthesis test platform for the aforementioned neuromuscular model is described and calibration procedures are reviewed. Next, the electromechanical limits of the prosthesis are analyzed and evaluated for the ability to produce biologic-like torque trajectories. System characterization of this platform is also reviewed, and a linear model of the system is presented.

In Chapter 5, the linear system model from Chapter 4 is used to design a force controller to enforce the target ankle behavior. A lead compensator is used in conjunction with feedforward terms and a positive torque feedback term to produce the desired torque-tracking performance.

In Chapter 6, the procedure for clinical tests on a bilateral amputee subject is described. The results of these trials are then presented.

Lastly, Chapter 7 summarizes the results and presents opportunities for future work.

2. Background

To best understand the control of a powered ankle-foot prosthesis, it is important to study the biomechanics of the normal human ankle during a walking gait cycle. This chapter provides a breakdown of the level-ground gait cycle and describes the basic functions provided by the human ankle during walking.

2.1. Normal Biomechanics of the Ankle-Foot Complex

Human walking is periodic in nature, and therefore may be analyzed using a representative period, called the gait cycle (GC). Normal human walking is typically analyzed for a single limb over the course of a single gait cycle. For level-ground walking, the gait cycle is usually defined as the period between successive heel-strikes of a given limb. The leg performs a variety functions over the course of this period, [13] but the analysis for the purposes of this thesis is restricted to the Sagittal plane.

In this thesis, the zero-degree angle (or neutral angle) of the prosthesis was defined as the point at which the shank of the leg is perpendicular to the bottom of the foot. Positive torque refers to that which, as applied by the ankle, tends to plantar flex the ankle (or "plantar flexion torque") as shown in Figure 2-1.

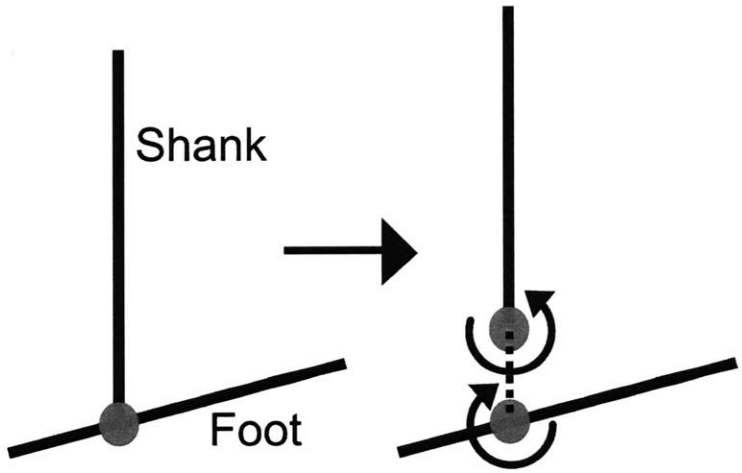

Figure 2-1: Positive ankle torque convention (Plantar flexion torque)

The gait cycle can be broken into two phases. The first phase of the gait cycle is the stance phase, (~60% of the GC) which is defined as the period of time when the foot is on the ground, from heel-strike to toe-off. In contrast, swing phase (~40% of the GC) is defined as the period of time when the foot is off the ground, from toe-off to heel-strike. The primary function of the ankle during the swing phase is to provide ground clearance by dorsiflexing the foot and returning the foot to the neutral position in preparation for the next heel-strike. As discussed in [1], the ankle behavior during this phase can be

modeled as a position control of the ankle joint around the state $\left[\theta = 0, \quad \dot{\theta} = 0\right]$, where θ and $\dot{\theta}$ are the ankle angle and angular velocity respectively.

To further describe the gait cycle, the stance phase can be broken into three sub-phases. These sub-phases are listed below, along with the primary function of the ankle-foot complex during each sub-phase [4].

- *Controlled Plantar flexion* (CP) occurs between heel-strike and foot-flat. During this phase, the ankle absorbs energy from the initial impact with the ground. Some of this impact energy is stored and the ankle helps pull the body center of mass forward over the foot. At foot-flat, the ankle joint angular velocity changes sign from negative to positive (plantar flexion to dorsiflexion).

- *Controlled Dorsiflexion* (CD) describes the period between foot-flat and maximum dorsiflexion. During this phase, the ankle slows the forward motion of the center of mass, and stores the energy for release later in the gait cycle. Maximum dorsiflexion is defined as the point in time during CD when the ankle joint angular velocity becomes negative (dorsiflexion to plantar flexion).

- *Powered Plantar Flexion* (PP) is the period when the ankle releases the energy stored from Controlled Dorsiflexion. The ankle provides energy in addition to this stored energy at moderate to fast walking speeds [6].

Figure 2-2 shows the progression of these phases of gait through one gait cycle.

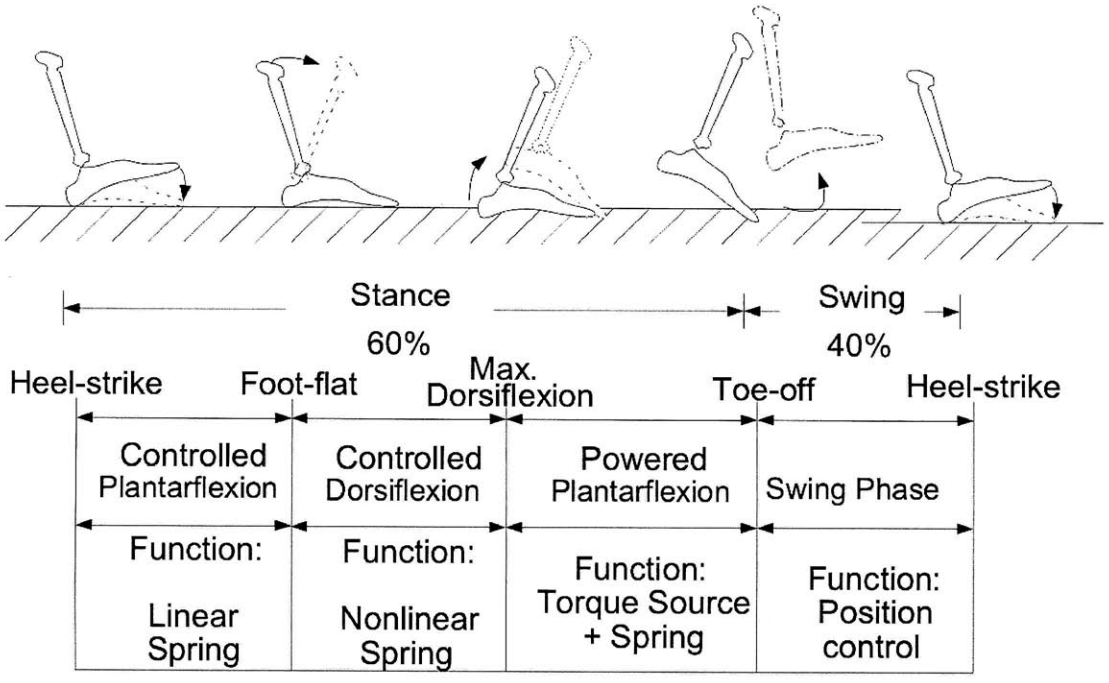

Figure 2-2: Gait cycle states (Source: [1])

When analyzing the ankle-foot complex for prosthesis control, it is often helpful to study the relationship between ankle torque and ankle angle graphically. An example of such a plot is shown in Figure 2-3.

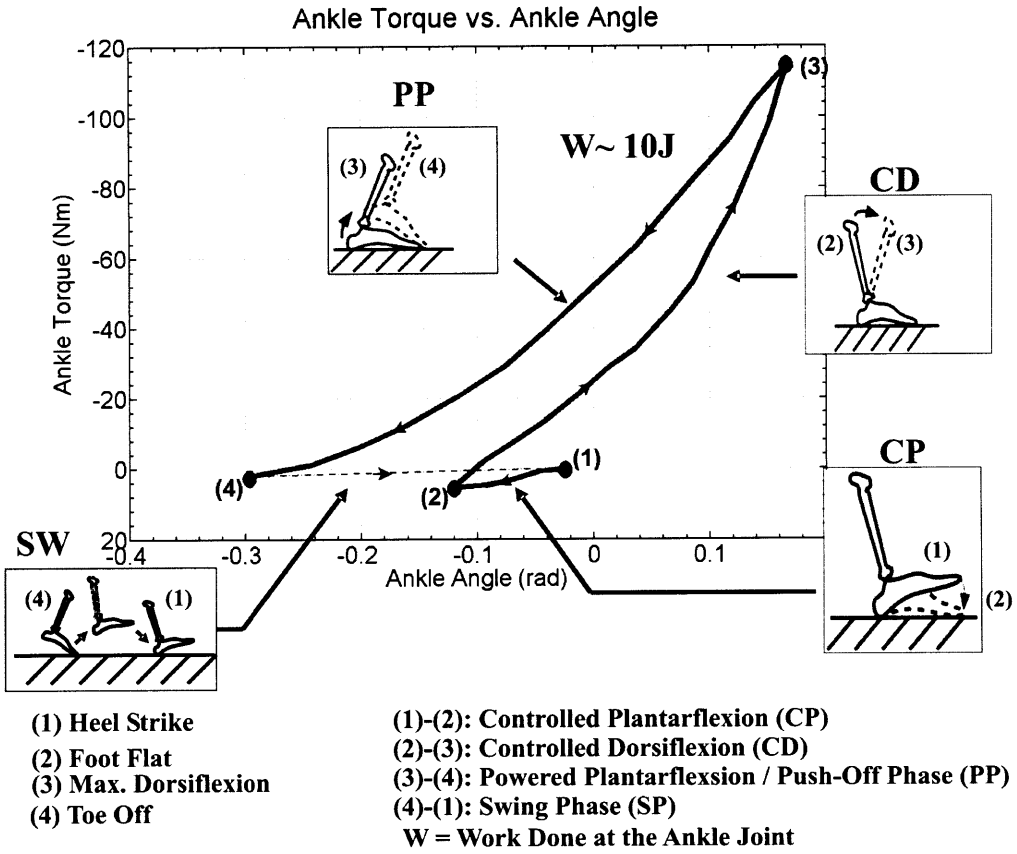

Figure 2-3: Ankle torque-angle relationship for a 75 kg subject at self-selected walking speed (1.25m/s) (source: [1])

Torque-angle curves are useful because they provide information about joint-stiffness and net work. The stiffness of the ankle at a given point in the gait cycle is the slope at the corresponding point on the curve. Furthermore, the net work can be calculated by integrating torque over angle, which is equal to the area inside the loop formed by the torque-angle curve (10 J in this case of Figure 2-3). The biological ankle typically exhibits an increase in stiffness at the transition from CP to CD (point 2), and an overall stiffness decrease at (point 3), as seen in Figure 2-3. The associated clockwise, and then counter-clockwise curves indicate energy storage during CD, followed by energy release during PP.

2.2. Discussion:

The gait cycle divisions described in this chapter aid in the analysis of human walking by dividing the gait cycle into manageable sections. In addition, the torque-angle plot provides a convenient way of graphically representing ankle positive net work and stiffness on a single plot. These tools are particularly useful for the development of powered ankle-foot prosthesis control systems. One can analyze the performance of a prosthesis and subsequently compare the results to those of the biological ankle. Such a process is followed in this thesis.

3. Desired Prosthesis Behavior

In an attempt to duplicate some of the functionality of the biological ankle-foot complex, this thesis used a neuromuscular model to provide the primary torque commands to a powered ankle-foot prosthesis. However, like the biologic counterpart, this muscle model is capable of simulating only unidirectional forces. Therefore, a unidirectional proportional-derivative (PD) impedance controller was used to provide the dorsiflexion commands to the prosthesis. A finite state machine (FSM) was employed to combine these two controllers into one that has the capability of producing bi-directional torque commands to the prosthesis. The dorsiflexor and plantar flexor were both connected to a two-link ankle-foot model to translate the forces from each modeled actuator into torques about the ankle joint. This chapter provides a detailed description of the dorsiflexor, plantar flexor, and finite state machine integration of these two controllers. The selection and optimization of the model parameters are also reviewed.

3.1. Finite State Machine

Given the highly repetitive nature of human walking and the well-defined phases in each gait cycle, (as detailed in Chapter 2), a finite-state machine (FSM) was chosen to handle the high level control of the prosthesis. This FSM was used to combine the unidirectional dorsiflexor and plantar flexor controllers into a single, bi-directional controller. In general, both the plantar flexor and dorsiflexor are enabled during the stance phase, whereas only the dorsiflexor is enabled during the swing phase of the gait cycle.

The state machine comprises five states. The *idle* and *init* states exist only for initialization and are therefore not discussed in this chapter. The *early-stance* (ES), *late-stance* (LS) and *swing* (SW) states, however, are traversed during normal use of the prosthesis, and are described in detail in this section. These three states represent the stages of the human gait cycle as described in Chapter 2. The SW state represents the swing phase of walking, whereas the combination of the ES and LS states represents the stance phase of walking. The primary purpose of this FSM is to distinguish between the stance and swing phase in real-time. The most direct way to distinguish between these two phases is to sense pressure on the sole of the prosthesis to determine if the prosthesis is on the ground. The prosthesis model used in this thesis lacked a pressure sensor, but it had previously been shown that the sign of the ankle torque was an effective indicator of heel-strike and toe-off transitions. The ankle torque was therefore used as the primary trigger for state transitions.

The state machine enters the SW state upon completion of the initialization steps. Almost all transitions between states thereafter are triggered by changes in ankle torque as measured by the set of strain gauges embedded in a prosthetic pyramid located at the top of the prosthesis (T_{py}). The state transition from the SW state to the ES (swing phase to stance phase) was defined as the point when the magnitude of T_{py} increased beyond the heel-strike threshold of 7 N·m of dorsiflexion torque ($T_{py} < -7$ N·m according to the convention) as applied by the ankle. This and all other transition thresholds were tuned

experimentally in previous clinical trials to minimize false transition triggers during level-ground walking while keeping the thresholds as small as possible.

The stance phase of walking is handled in the ES and LS states of the state machine. The two states exist as a way to split up the gait cycle in a similar manner as that described in Chapter 2, but for the purposes of prosthesis control. The slight differences in the handling of the ES and LS states become apparent in Chapter 5.

The state transition from ES to LS occurs approximately at foot-flat, when the ankle angle begins to increase, (motor angular velocity > 1 rad/s) and the ankle begins to produce plantar flexion torque of at least 12 N·m. Once in the LS state, the state can transition to SW only if the at some point in the LS state the measured torque exceeds 20 N·m and if the time passed in the LS state exceeds 200 ms. Both of these requirements for transition to the SW state were designed to prevent premature state transitions from swing through stance and back to swing. In addition to the above conditions, at least one of the two following conditions must also be met to enable the transition into the SW state from the LS state:

- *Torque Threshold*: The measured torque drops below 5 N·m,
- *Angle Threshold*: The ankle angle is plantar flexed by more than θ_{thresh} = 11 degrees. This transition condition was implemented to avoid Hall-effect angle sensor saturation during PP. (See Chapter 4 for more details on this sensor.)

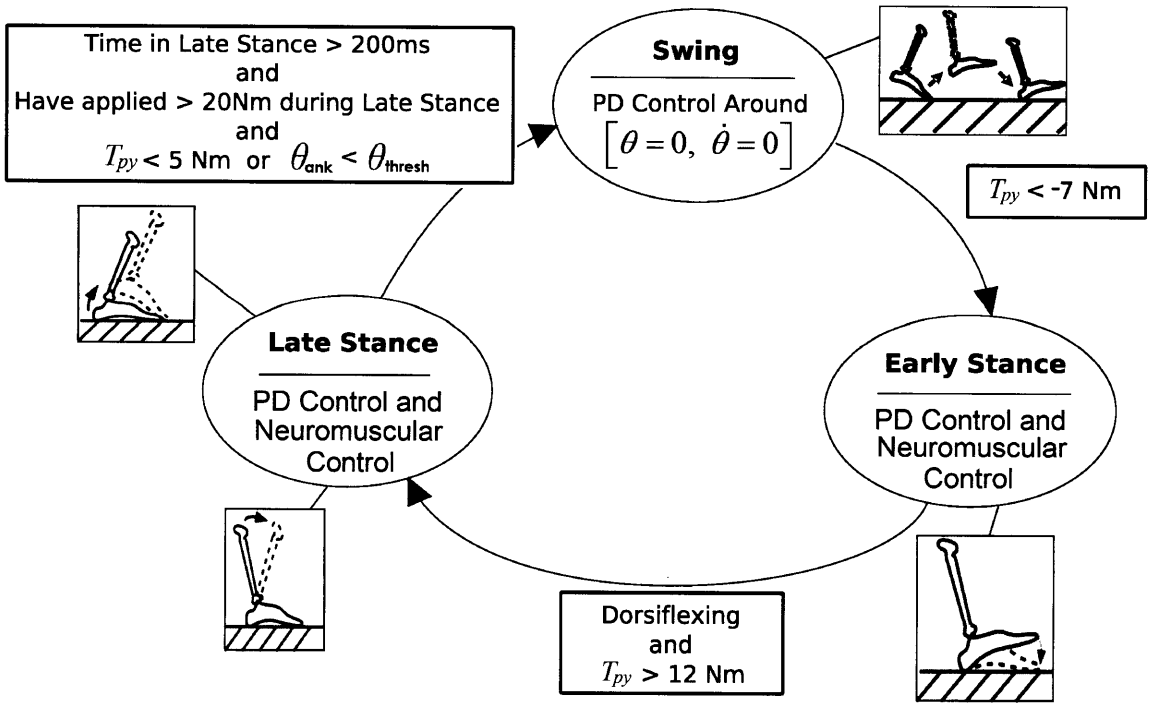

Figure 3-1: State Machine Diagram

The desired torque during both the ES and LS states is a sum of two counteracting elements. A unidirectional virtual spring-damper was implemented as a dorsiflexor for a two-link ankle-foot skeletal model, while a Hill-type model of an effective plantar flexor

muscle with positive force feedback (details in Section 3.2) was used as a plantar flexor for this ankle model (Figure 3-2). The combination of these two unidirectional elements provided the ability to command bi-directional prosthesis ankle torque during the gait cycle. Detailed descriptions of both of these elements are provided in the following sections.

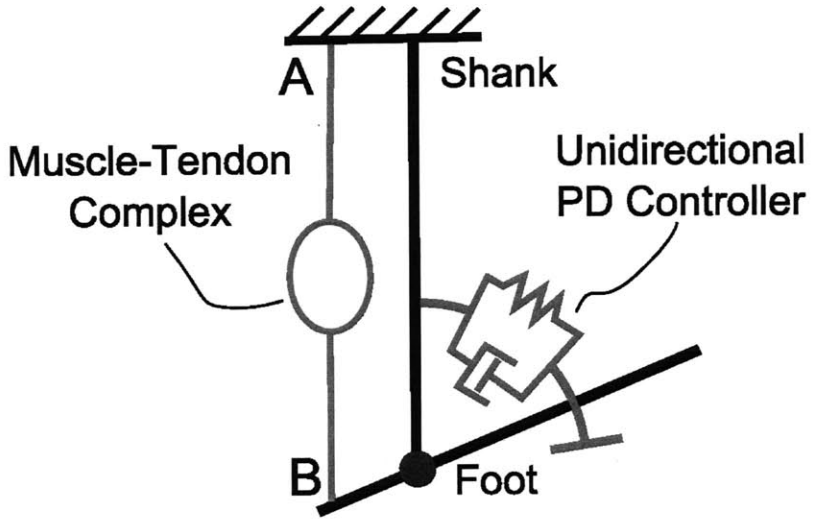

Figure 3-2 Hybrid control using a neuromuscular model (shown as muscle-tendon complex) and proportional-derivative impedance controller. The combination of these two unidirectional force sources allows for bi-directional torque commands to the prosthesis. The muscle model connects the heel of the foot to the shank at attachment points A and B.

3.2. Neuromuscular Model

There are a multitude of muscles responsible for ankle plantar flexion torque during human walking. Two muscles dominate in providing plantar flexion torque: the soleus and the gastrocnemius. The soleus, a monarticular muscle, acts only on the ankle joint, whereas the gastrocnemius, a biarticular muscle, has attachments at both the femur and heel. Force production of the gastrocnemius is therefore not only affected by the ankle joint state but the state of the knee joint as well. In this thesis, focus was limited to the ankle joint only. Therefore the muscle model used was based primarily upon the soleus. This effective muscle, however, also needed to incorporate the behavior of the many other plantar flexion muscles in the human calf. Thus, an optimization was performed to adjust select model parameters, as detailed in Section 3.4. The resulting muscle-model, incorporating a reflex loop for stimulation, was used as the primary high-level controller for ankle torque during the stance phase. The measured prosthesis ankle angle was used to determine muscle state, (see section 4.1 for more details on the sensors) and the resulting virtual muscle force was used as a component in determining the desired ankle

torque. In this section the muscle-model architecture and neural stimulation are described. The methods used for determining the effective muscle parameters are also reviewed.

The neuromuscular model (Figure 3-3) comprises a Hill-type muscle model, a neural-reflex loop, and a variable moment arm. The input to the model is ankle angle as measured by the prosthesis, and the output of the model is the muscle-model contribution to ankle torque. The model was based upon the architecture presented in [5], and modifications were made using the results in [Geyer, unpublished]. This section details each of the components of Figure 3-3.

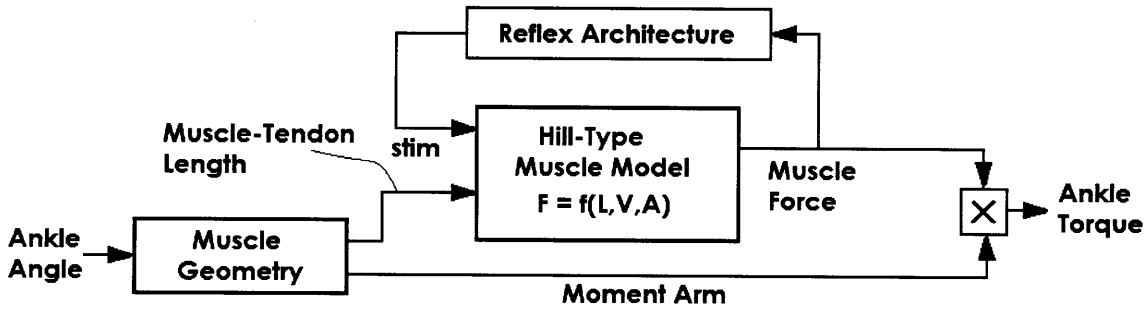

Figure 3-3: Neuromuscular model overall architecture.

3.2.1. Muscle Model:

At the core of the reflex muscle architecture is a Hill-type muscle model as seen in [5]. For simplicity, a single, effective muscle model was used to represent all of the major plantar flexor muscles in the human calf.

This Hill-type model [5] consists of a series-elastic element, (SE) which primarily models the Achilles tendon, and a contractile element (CE), which represents the active muscle fibers and associated elastic tissue. The elastic tissue, or parallel-elasticity (PE), comprises a high-limit parallel elasticity (HPE) and a low-limit parallel elasticity (LPE) (Figure 3-4). The elastic elements in this model were modeled as unidirectional springs to represent the fact that tendons generally cannot support significant compressive forces. (The LPE elasticity is an exception in that it can only support compressive forces by definition.) The elastic elements The entire structure combining the CE and SE is called the muscle-tendon complex (MTC) which connects to the heel of the foot and the shank as shown in Figure 3-2 at the attachment points *A* and *B* (Figure 3-4). All springs in this model are unidirectional, as indicated in Figure 3-4 by the one-way catches. Therefore, this plantar flexor muscle model can only be responsible for plantar flexion torques. Each element in the model is detailed in this section.

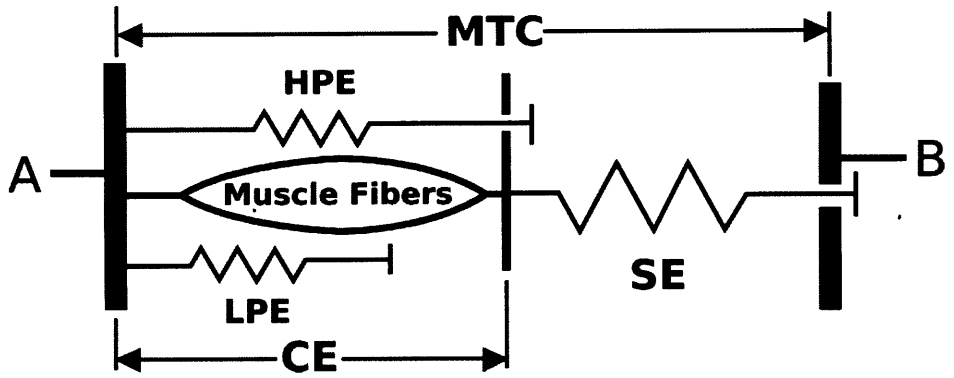

Figure 3-4: Architecture of the Hill-type muscle model used in this thesis [5]. The left and right ends (thick bars) attach to the heel and tibia in the two-link model.

The components of this muscle model are discussed in detail in the following three sub-sections.

3.2.1.1. Contractile Element Muscle Fibers

Human muscle exhibits large changes in force generation as its fiber length and contraction velocity change [9], [14]. In this Hill-type muscle model, CE muscle fiber force was modeled as a function of fiber length, velocity, and activation as follows: [5]

$$F_{MF}(l_{CE}, v_{CE}, t) = F_{\max} f_L(l_{CE}) f_V(v_{CE}) A(t) \tag{3.1}$$

where F_{MF} is the total force generated by the muscle fibers, $f_L(l_{CE})$ is the dimensionless force due to the muscle force-length relationship, $f_V(v_{CE})$ is the dimensionless force due to the force-velocity relationship, and $A(t)$ is the muscle activation ranging from 0 to 1. The product of these components is scaled by F_{max}, which is the muscle's maximum isometric force (Table 3-1).

The dimensionless force-length curve of the CE is a bell-shaped curve described by the following equation: [5]

$$f_L(l_{CE}) = \exp\left[c \left| \frac{l_{CE} - l_{opt}}{l_{opt} w} \right|^3 \right] \tag{3.2}$$

The optimum fiber length, l_{opt}, is the contractile-element length, l_{CE}, at which the muscle can provide maximum force under isometric conditions (F_{max}). Hence, the force-length curve is normalized such that $f_L(l_{opt})=1$. The parameter w is the width of the bell-shaped curve (Table 3-1), and the parameter c (Table 3-1) describes the shape of the curve by indicating the magnitude near to the extremes of the bell, where: [5]

$$f_L(l_{CE} = l_{opt}(1 \pm w)) = \exp(c). \tag{3.3}$$

The dimensionless force-velocity relationship of the CE is the Hill equation [9], and is described as follows: [5]

$$f_V(v_{CE}) = \begin{cases} \dfrac{v_{\max} - v_{CE}}{v_{\max} + Kv_{CE}}, & v_{CE} < 0 \\ N + (N-1)\dfrac{v_{\max} + v_{CE}}{7.56Kv_{CE} - v_{\max}}, & v_{CE} \geq 0 \end{cases} \tag{3.4}$$

Where v_{max} is the maximum contractile velocity of the muscle, v_{CE} is the fiber contraction velocity, K is the curvature constant (Table 3-1), and N (Table 3-1) defines the dimensionless muscle force (normalized by F_{max}) at the lengthening velocity $v_{CE} = -v_{max}$, such that: [5]

$$N = \frac{f_V(v_{CE} = -v_{\max})}{F_{\max}} \tag{3.5}$$

The contractile element activation, $A(t)$, is the muscle neural stimulation, STIM, fed through a low-pass filter of time constant τ as follows: [5]

$$\tau \frac{d(A(t))}{dt} = STIM(t) - A(t) \tag{3.6}$$

3.2.1.2. Contractile Element Parallel Elasticity (HPE, LPE)

There is typically some elastic behavior due to the tissues surrounding the contractile fibers. This elasticity acts in parallel with the contractile fibers, and engages when muscle fiber length exceeds some threshold. A parallel elasticity, modeled as a unidirectional nonlinear spring, was implemented for such a case. The force-length relationship for this high-limit parallel elasticity is shown in Eqn. (3.7) (Geyer, unpublished).

$$F_{HPE}(l_{CE}) = \begin{cases} F_{\max}\left(\dfrac{l_{CE} - l_{opt}}{l_{opt} w}\right)^2, & l_{CE} > l_{opt} \\ 0, & otherwise \end{cases} \tag{3.7}$$

It is also important to note that a low-limit parallel elasticity (LPE) was modeled in order to handle the possibility of the muscle-tendon complex becoming slack. A nonlinear spring was used of the form (adapted from Geyer, unpublished):

$$F_{LPE}(l_{CE}) = \begin{cases} F_{\max} \dfrac{\left[\dfrac{\left(l_{CE} - l_{opt}(1-w)\right)}{l_{opt}}\right]^2}{(w/2)}, & l_{CE} \le l_{opt}(1-w) \\ 0, & otherwise \end{cases} \cdot \tag{3.8}$$

3.2.1.3. Series-Elastic Tendon Model (SE)

A nonlinear spring was used as the series-elastic element (SE) and was meant to represent the Achilles tendon in the biological ankle. The normalized force of the spring F_{SE} was modeled a function of the spring length, as follows: [5]

$$F_{SE}(l_{SE}) = \begin{cases} F_{\max}\left(\dfrac{\varepsilon}{\varepsilon_{ref}}\right)^2, & \varepsilon > 0 \\ 0, & \varepsilon \le 0 \end{cases} \tag{3.9}$$

Where ε is defined as the tendon strain, [5]

$$\varepsilon = \frac{l_{SE} - l_{slack}}{l_{slack}} \tag{3.10}$$

and ε_{ref} is the reference strain (Table 3-1). Also, l_{slack} is the tendon slack length (Table 3-1) and l_{SE} is the tendon length. Since the tendon and muscle are in series with each other (Figure 3-4), the following equations hold: [5]

$$F_{CE} = F_{SE} = F_{MTC} \tag{3.11}$$

$$l_{MTC} = l_{SE} + L_{CE} \tag{3.12}$$

where F_{MTC} and l_{MTC} are the force and length of the muscle-tendon complex respectively. The muscle-tendon complex was modeled as the series combination of the contractile-element and series-elastic element [5].

Combining Eqns. (3.1), (3.7), (3.8), and (3.11) the behavior of the contractile element, parallel elasticity, and series elasticity can be fully described using the following equation:

$$F_{MTC} = F_{SE} = F_{CE} = F_{MF}(l, v, A) + F_{HPE} - F_{LPE} \tag{3.13}$$

A summary of the fixed (not optimized) musculoskeletal model parameters can be seen in Table 3-1. These values were based upon literature values or modified versions thereof [5].

3.2.2. Muscle Interaction

Now that the musculoskeletal model has been defined, the interaction of this model with its environment is now described. This interaction includes the mechanical connection between the muscle-tendon complex and the ankle joint (geometry) as well as the neural feedback to the muscle model.

3.2.2.1. Geometry:

Within the muscle model framework, the ankle angle, θ_{foot}, was defined as shown in the Figure 3-5.

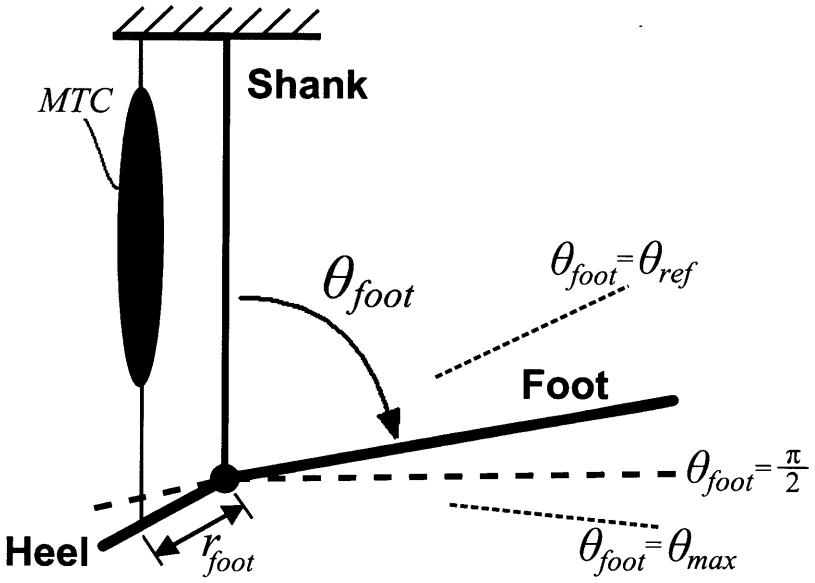

Figure 3-5 Muscle attachment model

According to Figure 3-5, the muscle-model ankle angle $\theta_{foot} = 0$, refers to the nonphysical condition when the foot is dorsiflexed by $\pi/2$ radians and is aligned with the leg shank. In contrast, plantar flexion of the ankle joint corresponds to an increase in θ_{foot}.

The muscle was modeled as an element parallel to the shank, attached to the tibia at one end. The heel-lever, r_{foot}, was defined as the radial distance from the ankle joint to the attachment point of the muscle. Also, a scaling factor, ρ, was introduced to account for the fact that the muscle fibers were modeled to lie at some non-zero angle to the muscle force vector.

A variable moment-arm was used to provide a relationship between θ_{foot} and F_{MTC} (Figure 3-5). A parameter ϕ_{max} was introduced to define the ankle angle at which the moment arm is at its maximum. This angle is not necessarily 90 degrees, as the heel-attachment lever may not be parallel to the foot itself (as shown in Figure 3-5). The component of ankle torque from the muscle model, $T_{ank,muscle}$, was obtained from the multiplication of the moment arm by the muscle force. Hence, Eqn. (3.14) defines the relationship between F_{MTC}, ankle torque and muscle-model ankle angle, θ_{foot}, as shown in Figure 3-5.

$$T_{ank,muscle} = F_{MTC}\cos(\theta_{foot} - \phi_{\max})r_{foot} \tag{3.14}$$

Given the ankle angle, the length of the muscle-tendon complex could also be obtained, using Eqn. (3.15)

$$l_{MTC} = [\sin(\phi_{ref} - \phi_{\max}) - \sin(\theta_{foot} - \phi_{\max})]r_{foot}\rho + l_{slack} + l_{opt} \tag{3.15}$$

where ϕ_{ref} is the reference ankle angle, as shown in Figure 3-5. The reference angle was defined as the angle at which $l_{CE} = l_{opt}$ and $l_{SE} = l_{\text{slack}}$. Both ϕ_{ref} and $\phi_{\max}$ were selected using the optimization discussed in Section 3.4.

3.2.2.2. Neural Control (Reflex Loop)

There are a multitude of possible neural control schemes for the Hill-type muscle model described in the preceding section. The muscle stimulation, *STIM(t),* can be determined from either an outside input or a local feedback loop. In this thesis, *STIM(t)* was obtained by using a local feedback loop, or "reflex architecture", namely a positive-force feedback framework, as developed in [5]. This neural-control was designed in [5] to mimic the stretch reflex in human muscle. A controller based on positive-force feedback as a neural control scheme has the advantage of not requiring a higher-level, external input to function. This controller is advantageous in prosthetics, since it requires no sensors external to the prosthesis.

In this architecture, the muscle force is delayed in time by $Delay_{RF}$ and scaled by a reflex gain, $Gain_{RF}$. This gained, delayed force is then introduced back into the muscle model as a stimulation signal, STIM, which is limited to range from 0 to 1. A pre-stimulation signal, *PRESTIM* is added to the stimulation to maintain a small level of muscle stimulation at all times. A diagram of this reflex architecture is shown in Figure 3-6 (based on [5]).

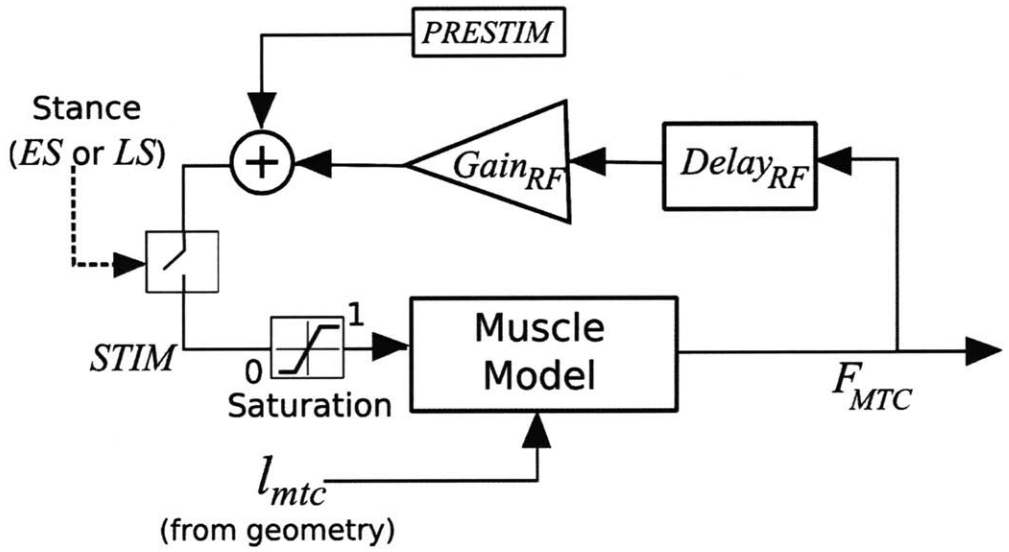

Figure 3-6: Reflex loop. (The muscle model shown here is the Hill-type model in Figure 3-4.)

As shown in Figure 3-6, during the SW state, the muscle stimulation is disabled in order to allow the dorsiflexor (Section 3.3) to act, thereby providing foot clearance in the swing phase. The implementation of the reflex loop in the neuromuscular model is shown in Figure 3-7.

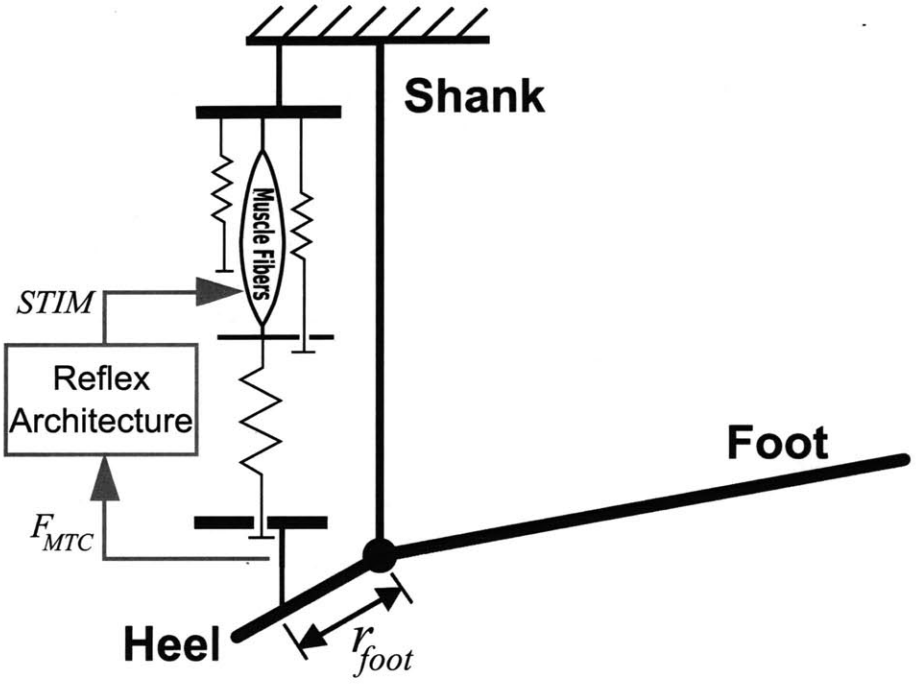

Figure 3-7: Neuromuscular model including positive force feedback as a reflex architecture. This figure summarizes the neuromuscular model described in Section 3.2

The following table contains the values of the fixed parameters of the neuromuscular model described in Sections 3.2.1 and 3.2.2.

Table 3-1: Parameter values (fixed) for the muscle model

l_{opt} [m]	0.04	w	0.56
l_{slack} [m]	0.26	c	ln(0.05)
v_{max} [l_{opt}/s]	6.0	N	1.5
ε_{ref}	0.04	K	5
PreA	0.01	ρ	0.5
T [s]	0.01	r_{foot} [m]	0.05
PreSTIM	0.01	$Delay_{RF}$ [s]	0.02

3.2.3. Implementation

For the muscle model described thus far to be useful in prosthetics, it must be implemented on the prosthesis microcontroller. Given the limited size and cost constraints in a robotic prosthesis, processing power is also limited. As a result, it is necessary to minimize computational costs of the model when it is implemented in software. Computationally, it is easier to simulate a model using integration than differentiation. Rather than numerically differentiating l_{CE} to obtain v_{CE} the force behavior of the model was used to back-calculate v_{CE} using the inverse of Eqn. (3.4), $v_{CE}(f_V)$. To obtain f_V, Eqns. (3.1) and (3.13) were re-arranged to obtain (Geyer, unpublished):

$$f_V = \frac{F_{SE} - F_{HPE} + F_{LPE}}{F_{\max} f_L A} \tag{3.16}$$

Since v_{CE} tends to be close to zero whenever the parallel elasticity is engaged, $f_V(v_{CE}\sim 0) = \sim 1$. Therefore, the approximation $F_{HPE} \sim f_V \cdot F_{HPE}$ was made. This approximation resulted in Eqn. (3.17) (Geyer, unpublished).

$$f_V = \frac{F_{SE} + F_{LPE}}{F_{\max} f_L A + F_{HPE}} \tag{3.17}$$

It is easier to implement Eqn. (3.17) than Eqn. (3.16) in simulation since Eqn. (3.17) avoids the numerically critical point when $F_{CE} \sim F_{HPE}$ ($A\sim 0$). Hence, given a known ankle angle θ_{foot}, the neuromuscular-model component of the ankle torque output can be calculated by combining Eqns. (3.9), (3.10), (3.11), (3.12), (3.15), and (3.17) to form:

$$F_{MTC} = F_{SE} = \begin{cases} F_{\max}\left[\dfrac{\left(l_{MTC}(\theta_{foot}) - l_{CE}\right) - l_{slack}}{l_{slack}}\right]^2, & \left(l_{MTC}(\theta_{foot}) - l_{CE}\right) > 0 \\ 0, & otherwise \end{cases} \tag{3.18}$$

where

$$l_{CE} = \int_0^t f_V^{-1}\left(\frac{F_{SE} + F_{LPE}(l_{CE})}{F_{\max} f_L(l_{CE}) A(t) + F_{HPE}(l_{CE})}\right) dt \,. \tag{3.19}$$

and f_V^{-1} is the inverse of Eqn. (3.4). Eqns. (3.18) and (3.19) can be numerically integrated, using Eqns. (3.8), (3.7), (3.2), (3.6) and (3.15) to obtain $F_{LPE}(l_{CE})$, $F_{HPE}(l_{CE})$, $f_L(l_{CE})$, $A(t)$, and $l_{MTC}(\theta_{foot})$ respectively, for a prescribed input trajectory, $\theta_{foot}(t)$. Eqn. (3.14) can then be used to determine $T_{ank,muscle}$ from F_{MTC}. The muscle model can therefore be treated as a system taking in a single input, $\theta_{foot}(t)$, and returning a single output, $T_{ank,muscle}$, provided that the muscle stimulation, $STIM(t)$, is determined from the reflex loop on F_{MTC}.

3.3. Dorsiflexor Model

As stated in Section 3.2.1, only one effective muscle was modeled. Therefore, only unidirectional force commands would be possible from the muscle model alone. For this reason, an effective dorsiflexor was needed in order to enable full control of the prosthesis. A proportional-derivative (PD) control law with a reference of $\left[\theta = 0,\ \dot{\theta} = 0\right]$ was implemented as a means providing dorsiflexion torque throughout the gait cycle. This control law (Eqn. (3.20)) provided the functionality of the Tibialis Anterior and other dorsiflexor muscles during the gait cycle.

$$T_{dorsi} = K_P\theta + K_V\dot{\theta} \tag{3.20}$$

Here, K_P is the proportional term (or spring constant in a virtual spring-damper model), whereas K_V is the derivative term (or the damping constant in a spring-damper model). Both of these terms are adjusted by the finite state machine depending on the state machine state, as follows:

Stance Phase:

The value of K_P during the stance phase was optimized along with some of the muscle model parameters to best match the model behavior to that of the biological muscle during normal level-ground walking (Section 3.4). The damping term was needed because it was found that, in the initial clinical trials, the forefoot would often bounce off of the ground at foot-flat. This bouncing behavior produced a momentary positive ankle

torque and triggered a premature state transition into the LS state. Therefore, K_V was experimentally tuned to 5 N·m·s/rad to dampen this behavior.

Swing Phase:

The primary function of the biological ankle during the swing phase, as discussed in Chapter 2, is to achieve ground clearance and to return the ankle angle to zero degrees in preparation for heel-strike. Therefore, the dorsiflexor was allowed to act bi-directionally during the swing phase and the proportional and derivative gains were set to 220 N·m/rad and 7 N·m·s/rad respectively. These gains were tuned experimentally in earlier prosthesis development for providing sufficiently fast dorsiflexion for ground-clearance early in the swing phase without sacrificing stability. However, the state machine was programmed to reduce the stiffness and damping of the PD control to match the values used during the ES and LS states whenever the time in the SW state (t_{SW}) exceeded 200 ms (approximately half the duration of the swing phase). This parameter change was implemented to avoid an abrupt impedance change at heel-strike.

Table 3-2: Summary of the dorsiflexor parameter values

State	ES, LS, SW($t_{SW} > 0.2$)	SW($t_{SW} < 0.2$)
K_P (N·m/rad)	(Optimized)	220
K_V (N·m·s/rad)	5	7

Since the dorsiflexor and neuromuscular model were expected to often be active simultaneously, a suppression gain, $Gain_{SUPP}$, was introduced to prevent the dorsiflexor from fighting the effective muscle during the stance phase. This gain served to reduce the torque resulting from the PD control law when the effective muscle accumulated force, as described by the relation, $\tau_{PDS} = \tau_{PD} - Gain_{SUPP} \cdot \tau_{NM}$, where τ_{PDS} is the suppressed dorsiflexor torque magnitude, τ_{PD} is the dorsiflexor torque magnitude before suppression, and τ_{NM} is the torque magnitude from the neuromuscular model. Once the dorsiflexor torque magnitude, τ_{PDS}, dropped to zero in a given stance phase, the dorsiflexor remained disabled for the remainder of the stance phase to prevent it from fighting the neuromuscular model in terminal stance. More details about the selection of $Gain_{SUPP}$ can be seen in section 3.4.

3.4. Parameter Optimization:

The majority of the parameters in the muscle model was based on literature values of human muscle, or slightly modified versions of said values [5] as shown in Table 3-1. The soleus was chosen as a reference to obtain these parameters because it is the primary monarticular source of plantar flexion torque during normal level-ground walking. However, the accurate measure of some parameters, such as $F_{max,}$ and $Gain_{RF}$, pertaining to the grouping of the individual muscles, was not available from literature. It was suggested to select these unknown values such that the behavior of the walking model would best match that of the biological system. A parameter optimization was therefore performed to match the ankle torque profile generated by the model to that of the

biological ankle of a human subject for a given input ankle angle profile. The optimized system comprised the entire hybrid controller as described in Sections 3.1 through 3.3. The input to the model was ankle angle, and the output was total ankle torque (the combination of the neuromuscular torque and the impedance controller torque).

3.4.1. Optimized Parameters

The following parameters were chosen for tuning: F_{max}, $Gain_{RF}$, $Gain_{SUPP}$, ϕ_{ref}, and ϕ_{max}. A genetic algorithm optimization was chosen to cover the search space and handle possible discontinuities in the fitness function when performing this initial search. A direct search was combined with the genetic algorithm to pinpoint local minima in the fitness landscape. The Genetic-Algorithm tool in Matlab was used to implement both optimization methods. (See Appendix A for information on optimizer settings.) Level-ground human walking data (Section 3.4.2) at two different speeds were used to provide the reference behavior for the optimization. The neuromuscular model parameters were optimized separately for each of these two walking speeds, hence leading to two parameter sets. The allowable range for each of the optimization parameters can be seen in Table 3-3.

Table 3-3: Optimization Parameter Ranges

Parameter (Units)	Minimum Value	Maximum Value
F_{max} (N)	3000	7000
$Gain_{RF}$	0.6	1.5
K_P (N·m/rad)	20	250
$Gain_{SUPP}$	0	5
ϕ_{ref} (rad)	0.5236	2.0944
ϕ_{max} (rad)	1.3963	2.4435

The initial population was chosen by the optimizer.

3.4.2. Target Behavior:

Kinetic and kinematic walking data were collected at the Gait Laboratory of Spaulding Rehabilitation Hospital, Harvard Medical School, in a study approved by the Spaulding committee on the Use of Humans as Experimental Subjects [7]. A healthy adult male (81.9 kg) was asked to walk at slow and self-selected walking speeds across a 10m walkway in the motion capture laboratory after informed consent was given.

The motion-capture was performed using a VICON 512 motion-capture system, comprising eight infrared cameras. Reflective markers were placed at 33 locations on the subject's body in order to allow the infrared cameras to track said locations during the trials. The cameras were operated at 120 Hz and were able to track a given marker to within approximately 1mm. The markers were placed at the following bony landmarks for tracking the lower body: bilateral anterior superior iliac spines, posterior superior iliac

spines, lateral femoral condyles, lateral malleoli, forefeet and heels. Wands were placed over the tibia and femur, and markers were attached to the wands over the mid-shaft of the tibia and the mid-femur. Markers were also placed on the upper body at the following sites: sternum, clavicle, C7 and T10 vertebrae, head, and bilaterally on the shoulder, elbow, and wrist joints.

Ground reaction forces were measured using two staggered force plates (model no. 2222 or OR6-5-1, by Advanced Mechanical Technology Inc. Watertown, MA, USA), which were incorporated into the walkway. The precision of these force plates in measuring ground reaction force and center of pressure is approximately 0.1 N and 2 mm respectively. The force plate data was collected at 1080 Hz and synchronized with the VICON motion capture data.

Joint torques were calculated from the ground reaction forces and joint kinematics using a modified version of a standard inverse dynamics model. Vicon Bodybuilder, by Oxford Metrics, UK was used to perform the inverse dynamics calculations.

The target ankle and torque trajectory at the moderate, level-ground, walking speed was obtained from an average of 5 gait cycles at the subject's self-selected speed (1.28 m/s mean). Six trials were obtained for the slow level-ground walking speed (1.04 m/s mean). A single trial was selected from these six trials as a test of the controller's capability at this slower speed. The time-history average profiles and target profiles for ankle angle and torque can be seen in Figure 3-8, Figure 3-9, Figure 3-10, and Figure 3-11. The end of the stance phase was defined as the point in time when the joint torque first dropped to zero after the peak torque was reached in the gait cycle. This event occurred at 63% gait-cycle for the moderate walking speed, and 67% gait-cycle for the slow walking speed.

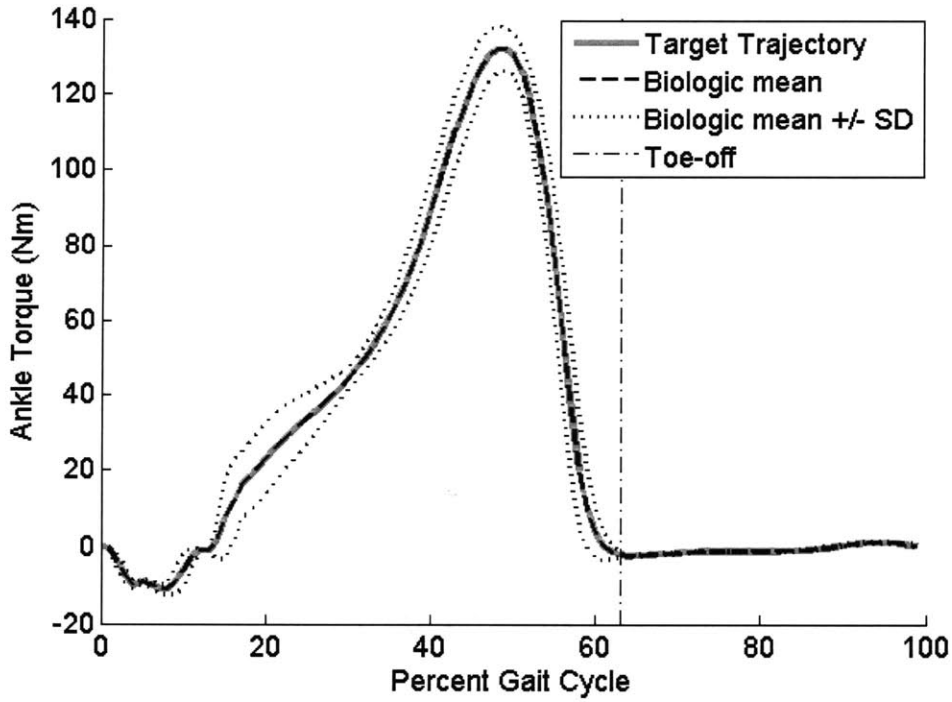

Figure 3-8: Biological ankle torque profile vs. time (moderate speed: 1.28 m/s)

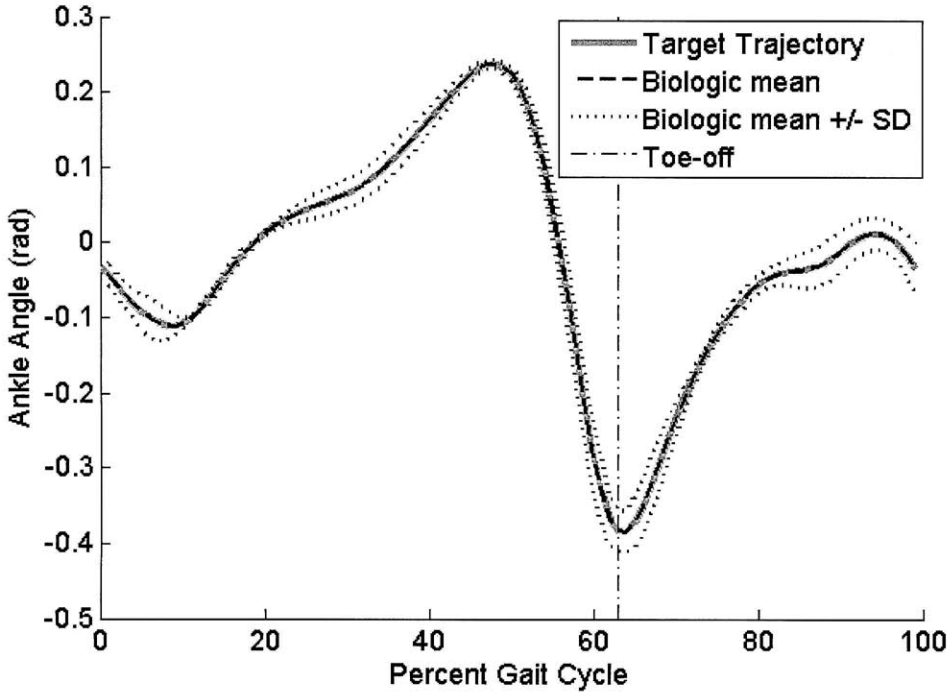

Figure 3-9: Biological ankle angle profile vs. time (moderate speed: 1.28 m/s)

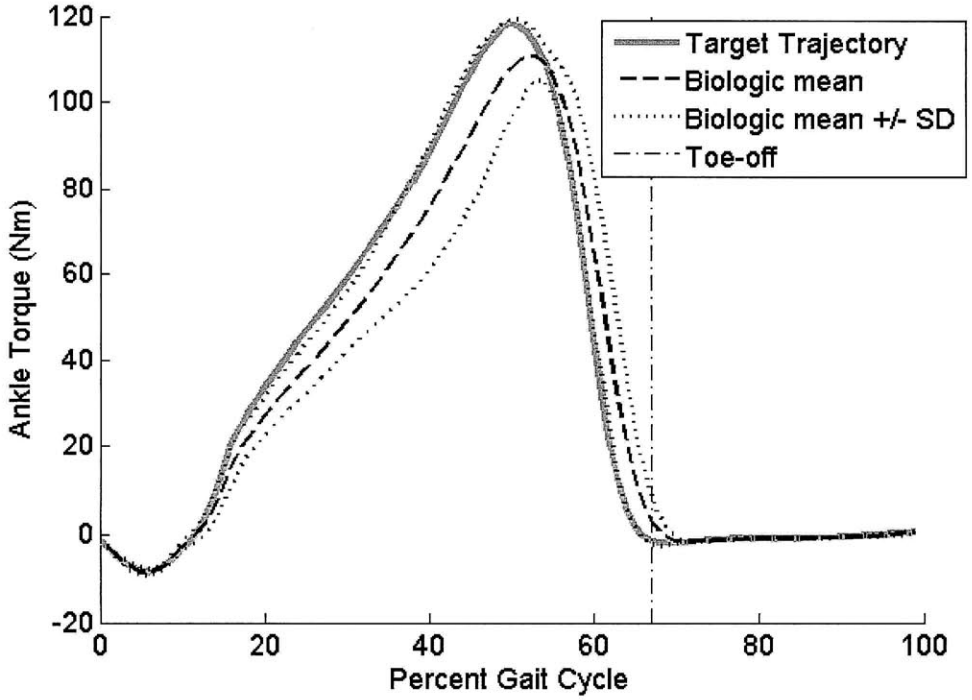

Figure 3-10: Biological ankle torque vs. time (slow speed: 1.04 m/s)

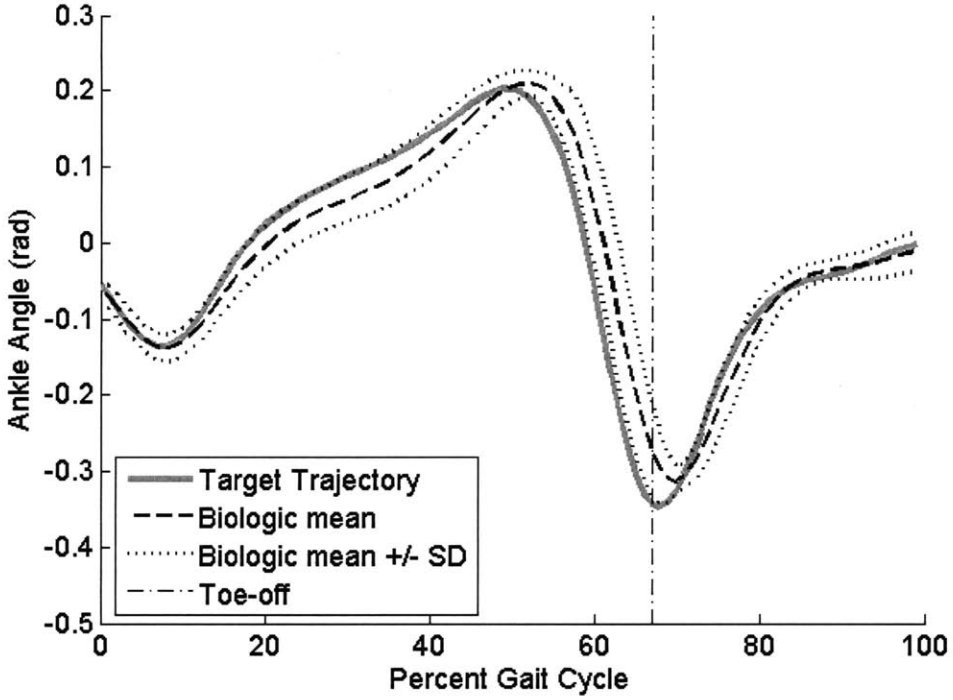

Figure 3-11: Biological ankle angle vs. time (slow speed: 1.04 m/s)

3.4.3. Cost function:

The biological ankle angle and ankle torque trajectories shown in Section 3.4.2 were used as the target ankle behavior for the optimization. The cost function for the optimization was defined as the squared error between the biologic and simulation torque profiles during the stance phase, given the biological ankle angle trajectory, i.e.:

$$Cost = \sum_{t \in STANCE} \left(T_{sim}(t) - T_{bio}(t) \right)^2 \tag{3.21}$$

where T_{sim} is the torque output of the simulation, T_{bio} is the biological ankle torque, and θ_{bio} is the biological ankle angle for the given walking speed.

3.4.4. Results

A set of parameters was obtained for each of the two walking speeds using the optimization method from Section 3.4.1. Table 3-4 summarizes these two parameter sets.

Table 3-4: Optimization Results - Parameter Sets

	Moderate Speed	Slow Speed
F_{max} (N)	3312	3377
$Gain_{RF}$	1.188	1.225
K_P (N·m/rad)	104.9	72.9
$Gain_{SUPP}$	0	0
ϕ_{ref} (rad)	1.663	1.492
ϕ_{max} (rad)	1.852	1.951

As a verification of the optimization effectiveness, a simulation of the combined neuromuscular model and impedance controller was run with the final parameters for each walking speed using the biological ankle angle at each speed as input to the model. The resulting torque profiles were compared to the biologic torque profiles as shown in Figure 3-12 and Figure 3-13.

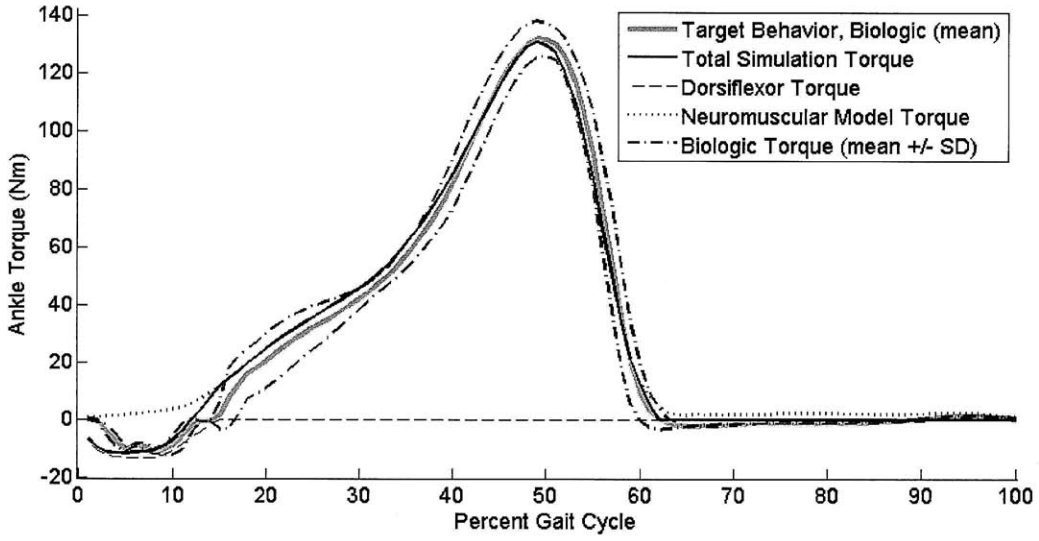

Figure 3-12: Optimization vs. biologic torque (moderate speed) showing components of optimization torque

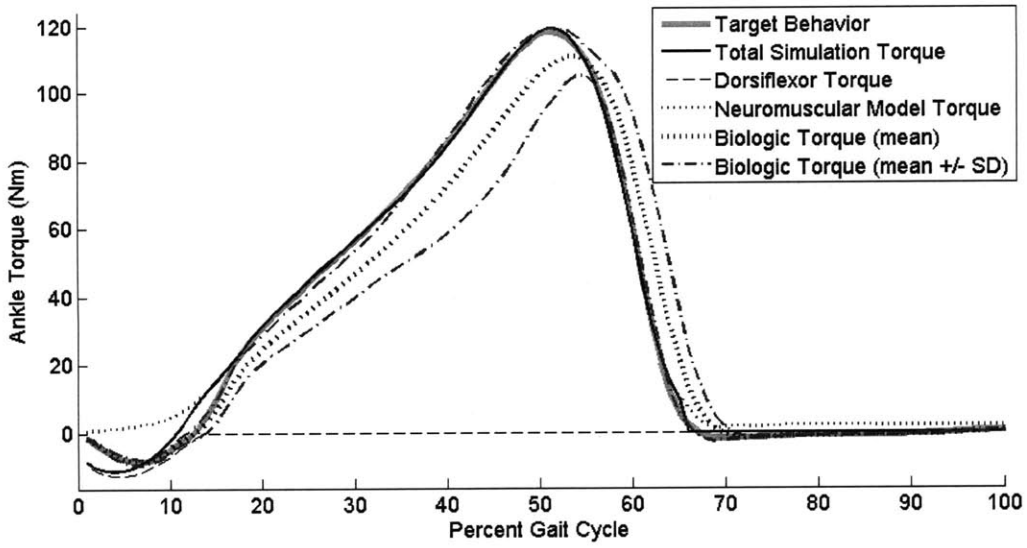

Figure 3-13: Optimization vs. biologic torque (slow speed) showing components of optimization torque

From Figure 3-12, it is clear that the simulated torque trajectory remains within the biologic standard deviation envelope for most of the gait cycle. This result indicates a high correlation between the simulated and target (mean) trajectories. Similar tracking of the simulation to the target trajectory is shown in Figure 3-13, although in this case the target trajectory itself does not lie at the center of the standard deviation envelope.

The discrepancy between the simulation and biologic data during controlled plantar flexion is most likely a result of the implementation of the impedance controller as a dorsiflexor. If, instead, an additional neuromuscular model was used to implement the dorsiflexor, the availability of more tunable parameters would likely lead to a better correlation in behavior with the biological ankle. However, for simplicity, the proportional-derivative controller was used as the dorsiflexor for this study. The fact that the suppression gain $Gain_{SUPP}$ was optimized to zero indicates that the muscle model inherently suppresses the dorsiflexor during stance by overpowering it until the impedance controller torque drops to zero.

3.5. Summary

In this chapter, a hybrid ankle-foot prosthesis controller comprising a neuromuscular model and proportional derivative impedance controller was developed. The ankle torque-angle relationship of a human with intact limbs walking on level-ground was used as the target for an optimization of select model controller parameters at two different walking speeds. The resulting optimized controller was able to closely mimic the biological ankle torque when the biological ankle angle profile was given as an input. Therefore, it was expected that this controller, if implemented on a prosthetic ankle, could produce biologically-consistent ankle torques provided that the biological ankle trajectory was enforced. However, before clinical trials with a robotic prosthesis were performed to validate this hypothesis, it was first necessary to ensure that the prosthesis was capable of producing the desired biological torques. The next chapter details the tests performed to evaluate the capabilities of the prosthesis hardware.

4. Mechanical Analysis

A powered ankle-foot prosthesis was used as a test platform for the evaluation of the neuromuscular architecture discussed in Chapter 3. It was necessary for the purposes of the study to assess the ability of the prosthesis to produce biologic-like torques for level-ground walking while being worn by an amputee. This chapter first provides an overview of the electromechanical system. Next, a simplified system model is presented. The calibrations performed on the prosthesis are detailed, and the performance-limiting characteristics of this system are analyzed. The chapter concludes with the presentation of a system characterization method for obtaining model parameters and the resulting characterized system. The implications for prosthesis control are then discussed.

4.1. Physical System

The mechanical system comprises a series-elastic actuator, (SEA) which includes a DC electric motor, transmission, and a spring in series with the aforementioned drive train. In addition, a unidirectional parallel spring engages for ankle angle $\theta > 0$, and provides plantar flexion torques in parallel with the actuator. Strain gauges, mounted both on the series spring and on the prosthetic pyramid at the top of the prosthesis housing, provide estimates of drivetrain torque and ankle torque respectively. An optical encoder connected to the motor shaft provides an approximate measure of ankle joint angle. In addition, a Hall-effect sensor at the ankle joint provides a more direct measurement of ankle angle. The physical system can be seen in Figure 4-1.

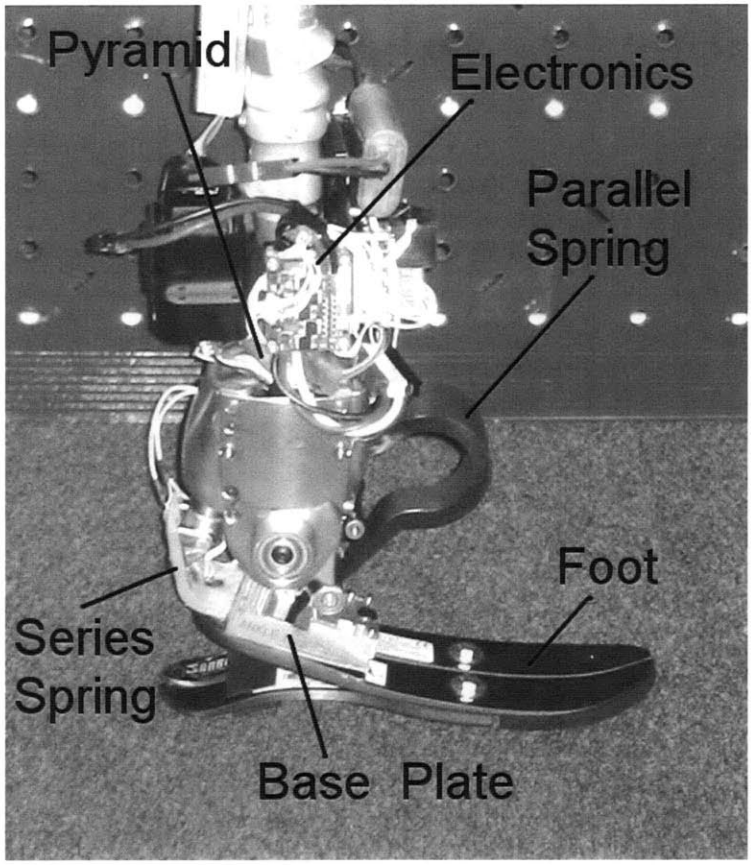

Figure 4-1: Physical system

A Maxon Powermax 200 Watt Ec-30 48V brushless motor [17] drives a 3 mm-pitch linear ballscrew through a 40/15 gear-ratio timing belt pulley system (Figure 4-2). Movement of the ballscrew translates to angular rotation of the ankle joint through the series spring, a bent piece of Kevlar-fiber composite attached to the ball nut at a clevis. A steel parallel leaf spring protrudes from the front of the prosthesis. This leaf spring presses against the front ramp (Figure 4-2) for ankle angles $\theta > 0$ using a bearing. The physical parameters of the prosthesis are summarized in Table 4-1.

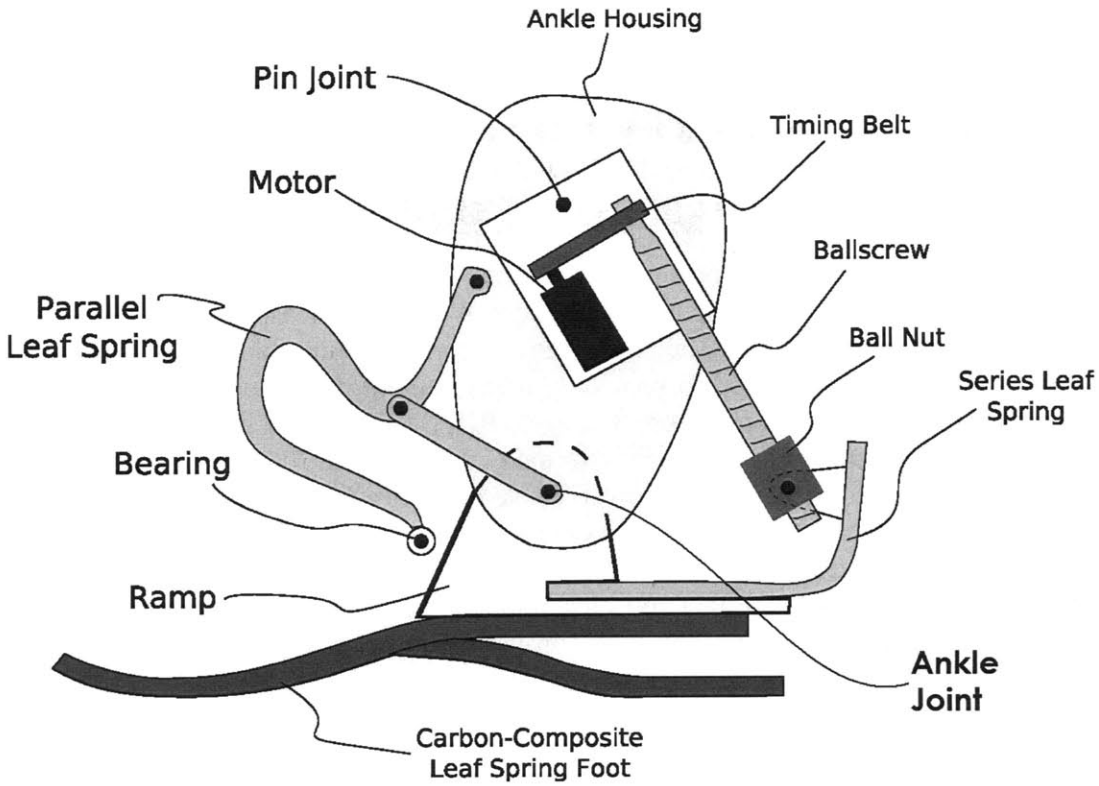

Figure 4-2: Simplified diagram of the test platform

When the ballscrew pulls up on the series spring, as seen in Figure 4-3, a moment is applied to the spring about point C. However, when the direction of applied ballscrew force is reversed, the moment applied to the series spring becomes smaller, due to the greater proximity of point D to the force vector. This change in moment arm results in a direction-dependent series spring stiffness. The designed stiffness is 1200 N·m/rad for providing dorsiflexion ankle torque, but 533 N·m/rad for providing plantar flexion ankle torque.

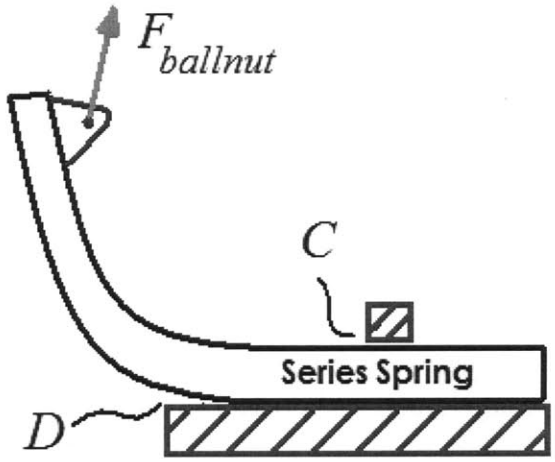

Figure 4-3: Diagram of Series Spring

A standard prosthetic pyramid installed 82 mm above the ankle joint pivot houses a set of strain gauges which were used to estimate the total joint torque. This torque measurement, however, is only an approximation, since any Sagittal plane shear force, F_{shear}, applied to the shank contributes to the measured moment by $F_{shear}*r_{py}$ where r_{py} is the distance from the ankle joint to the strain gauges. Therefore, the pyramid strain gauge measurement was used only as a trigger for the state transitions, as discussed in Chapter 3.

An optical encoder is located on the motor to enable the precise measurement of motor rotation. However, as discussed in Section 4.3.2, this measurement cannot be used to reliably measure the angle at the ankle joint. A combination of a Hall-effect sensor and bar magnet was therefore used to provide a measurement of ankle angle. However, this sensor has a limited angle range from $\theta_{min,Hall}$ to $\theta_{max,Hall}$ (Table 4-1).

The prosthesis is controlled by two dsPIC33FJ128MC706 microcontrollers. One microcontroller is connected to a power electronics circuit board and acts as a motor controller. This microcontroller implements a feedback control loop on motor current. The other microcontroller executes the high-level algorithms, which, for this study included the state-machine and muscle model. For this thesis, motor current was software-limited to ±25 Amps, the main program loop rate was set to 500Hz, and the motor controller pulse width modulation frequency was fixed at 100 kHz.

Table 4-1: Powered ankle-foot prosthesis specifications

I_m	33.3 g·cm^2
K_t	2.76e-3 N·m/A
R	200
K_s **(dorsiflexion torque)**	1200 N·m/rad
K_s **(plantar flexion torque)**	533 N·m/rad
$\theta_{max,Hall}$	0.1571 rad (9 deg)
$\theta_{min,Hall}$	-0.192 rad (-11 deg)
Main Loop Sample Rate (Hz)	500
Pulse-Width-Modulation Rate (kHz)	100
Max Motor Current Command (Amps)	25

4.2. System Model

For the purposes of this thesis, a linear lumped-parameter model was used to represent the powered prosthesis, as in [1]. For simplicity, the following assumptions were made:

- Neglect nonlinearities such as stick-slip friction and backlash.
- The transmission ratio does not change with ankle angle.
- The foot plate and ankle shank are of negligible inertia compared to the relatively large effective motor inertia as seen through the drive train.

The motor was modeled as a torque source acting on the motor inertia, I_m, with motor damping B_m. This motor was modeled in series with a spring of rotary stiffness K_s through a transmission of gear ratio R. The lumped-parameter model is shown in Figure 4-4.

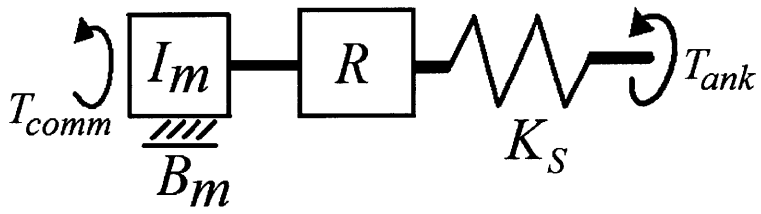

Figure 4-4: Lumped-parameter model for the prosthesis drive train

Since torque production was the primary concern, the case when both ends of the prosthesis are fixed was considered, as described in [1] and shown in Figure 4-16. The equivalent inertia, I_e, and equivalent damping, B_e, as seen at the ankle joint were then found using the equations for the rotational equivalent of the model from [1].

First, the motor inertia seen through the drive train was approximated using the equation:

$$I_e \approx R^2 I_m \tag{4.1}$$

resulting in a value of $I_e = 0.1332$ kg·m^2. Likewise, the equivalent damping at the ankle joint was related to the motor damping using:

$$B_e = RB_m . \tag{4.2}$$

The second-order model for the torque at the ankle joint was then,

$$\frac{\mathrm{T}_{ank}}{\mathrm{T}_e} = \frac{K_s}{I_e s^2 + B_e s + K_s} . \tag{4.3}$$

where T_{ank} is the torque seen at the ankle joint. The effective commanded ankle torque, T_e, was related to the commanded motor current, i_{comm}, using equation (4.4),

$$T_e = RT_{comm} = RK_t i_{comm} \tag{4.4}$$

where K_t (Table 4-1) is the motor torque constant.

The remainder of this chapter describes how the model parameters I_e, B_e *and* K_s were evaluated, and discusses the capability of the prosthesis of producing biologic torque levels.

4.3. Sensor Calibration

Prior to performing any meaningful physical system analysis, calibration of the sensors on the prosthesis was required. Therefore, the following analyses were performed.

4.3.1. Pyramid and Series Spring Strain Gauge Calibration

The carbon-composite foot was removed from the bottom of the prosthesis, and the base plate was screwed rigidly to the mounting platform shown in Figure 4-5. This platform was, in turn, mounted rigidly to a workbench such that the shank of the prosthesis was horizontal and the toe was pointed towards the ground. A ~1 m pole was attached to the shank to provide a large moment arm by which to apply torque about the ankle joint. An impedance controller was activated such that the commanded prosthesis torque followed the control law defined by Eqn. (4.5).

$$T_{comm} = K_{cal}(\theta - \theta_{ref}) + B_{cal}(\dot{\theta} - \dot{\theta}_{ref}) \tag{4.5}$$

The reference angle θ_{ref} was set to approximately -0.23 radians (plantar flexed) from the engagement of the parallel spring and the reference velocity, $\dot{\theta}_{ref}$, was set to zero. The angle offset was needed to ensure that the parallel spring did not engage so that all applied force was transmitted through the series spring. The proportional term, K_{cal}, and the derivative term, B_{cal}, were set to relatively high values of ~600 N·m/rad and ~7 N·m·s/rad respectively. This high impedance was necessary to prevent very large deflections from the reference angle since such high deflections would likely result in engagement of the parallel spring.

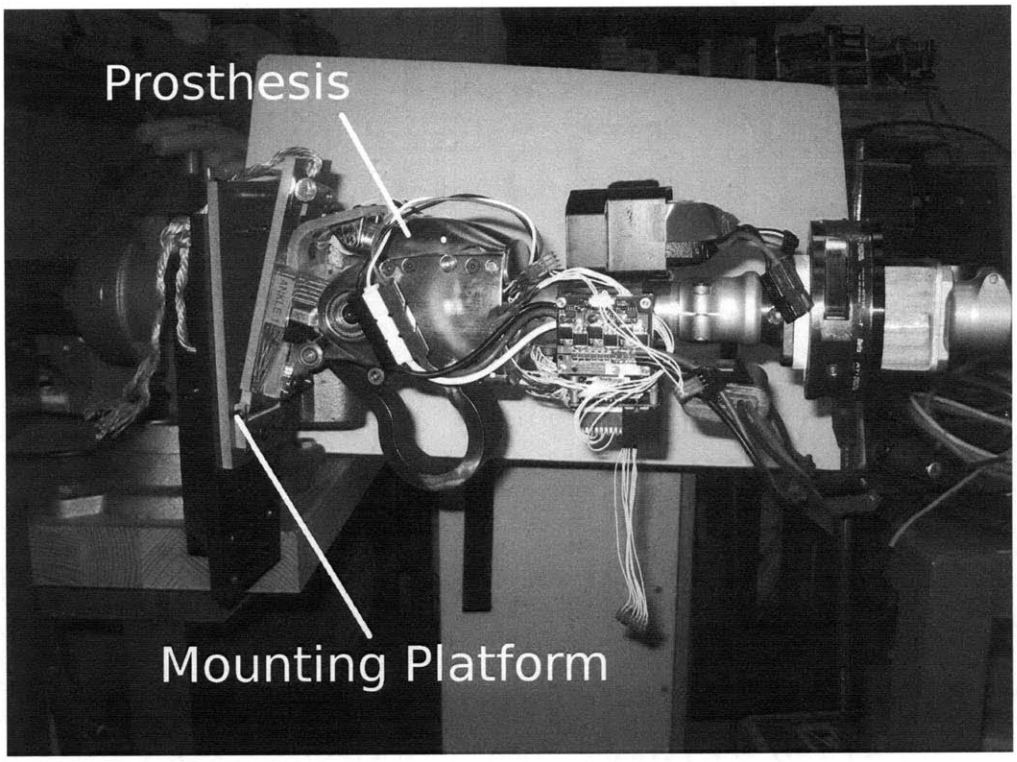

Figure 4-5: Strain Gauge Calibration Setup

Known weights were hung from known locations along the pole so to apply varying amounts of shear forces and moments to the ankle joint. The weights were hung in 11-kg increments, starting from 11 kg and increasing to 33 kg. For each weight hung, the moment arm was increased monotonically across five values ranging from 0.108 m to 0.418 m, with the exception of the 33 kg weight, for which the longest moment-arm was omitted. The output from the strain gauges was noted for each of the weight-moment arm pairs, and a linear fit to the data was found. This linear fit, along with the data points, can be seen in Figure 4-6. In the linear fit, only the slope was used for the strain gauge calibration, since any torque offset could be zeroed prior to tests. The same linear curve-fit was also performed for the series spring strain gauge, (Figure 4-7) since all of the applied ankle torque, excluding minor frictional losses, was transmitted through the series spring. As a check, the ankle angle with respect to the horizontal was estimated by the motor encoder. This angle was used to provide a more accurate calculation of applied force, using $F_{applied} = mgcos(\theta)$, where m is the mass of the weight hung, g is gravitational acceleration, and θ is the shank angle from the horizontal. However, due to the setup, the shank angle from the horizontal was bounded by 0.227 radians (13 degrees) and ended up being much less than 0.227 once loading began. Therefore, the angular correction factor provided little contribution to the calibration accuracy.

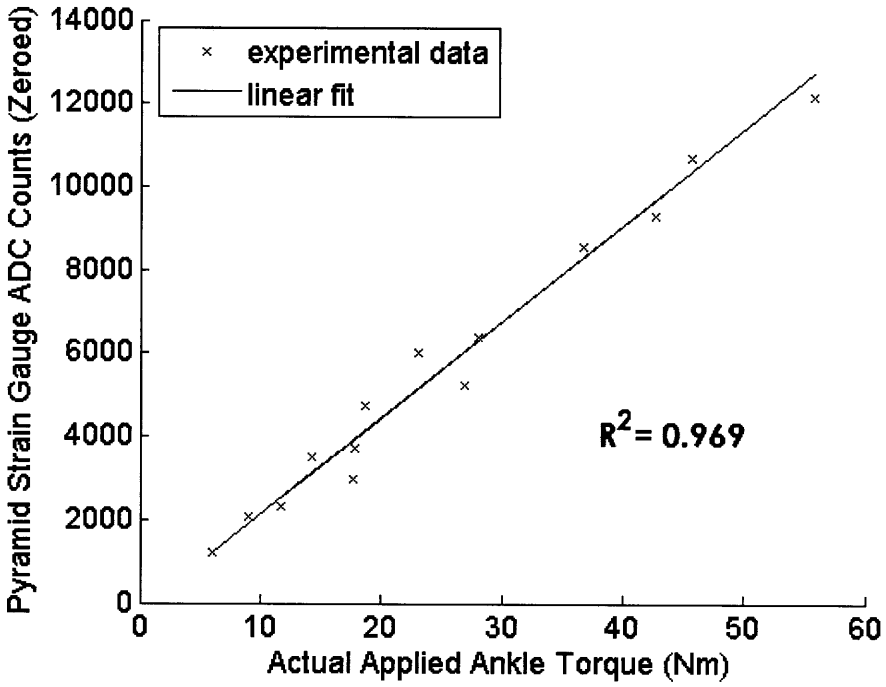

Figure 4-6: Pyramid strain gauge torque calibration

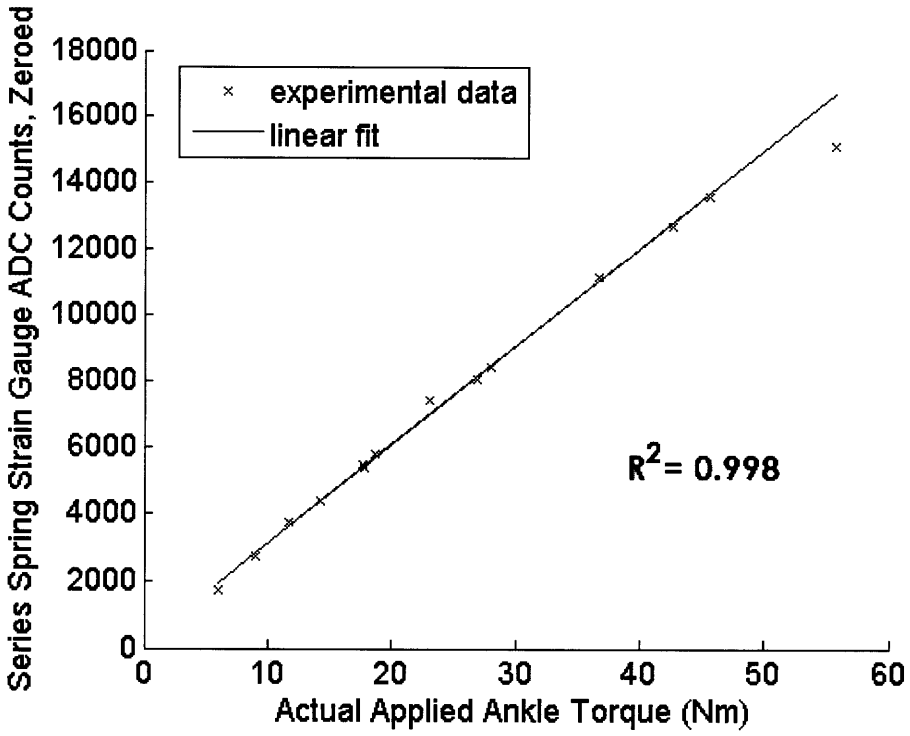

Figure 4-7: Series spring strain gauge torque calibration

This torque calibration was performed only for positive (plantar flexion) ankle torque, since positive torque is developed for most of the stance phase (Figure 3-8, Figure 3-10). It was assumed that the linear fit would apply for the application of negative (dorsiflexion) torque.

4.3.2. Hall-Effect Angle Sensor Calibration

The presence of the series spring between the motor and the ankle joint breaks the direct relationship between motor angle and output ankle angle when non-zero drive train forces develop. As a result, the motor encoder cannot provide a consistently accurate measure of ankle angle. A Hall-effect sensor was therefore included in the mechanical design of the prosthesis for measuring the ankle angle directly. Calibration of this sensor was performed using the motor encoder while drive train forces were kept low.

During the calibration, zero motor current was commanded to minimize forces in the drive train and hence the series spring. Given the small forces involved, (most due to coulomb friction) the motor encoder could be used to calibrate the Hall-effect sensor with minimal error. The ankle joint was moved through its range while recording both the Hall-effect sensor angle output and the motor encoder output. As a repeatability check, the ankle angle was moved in a random pattern to cover a large state space. The resulting comparison between the two sensors may be seen in Figure 4-8.

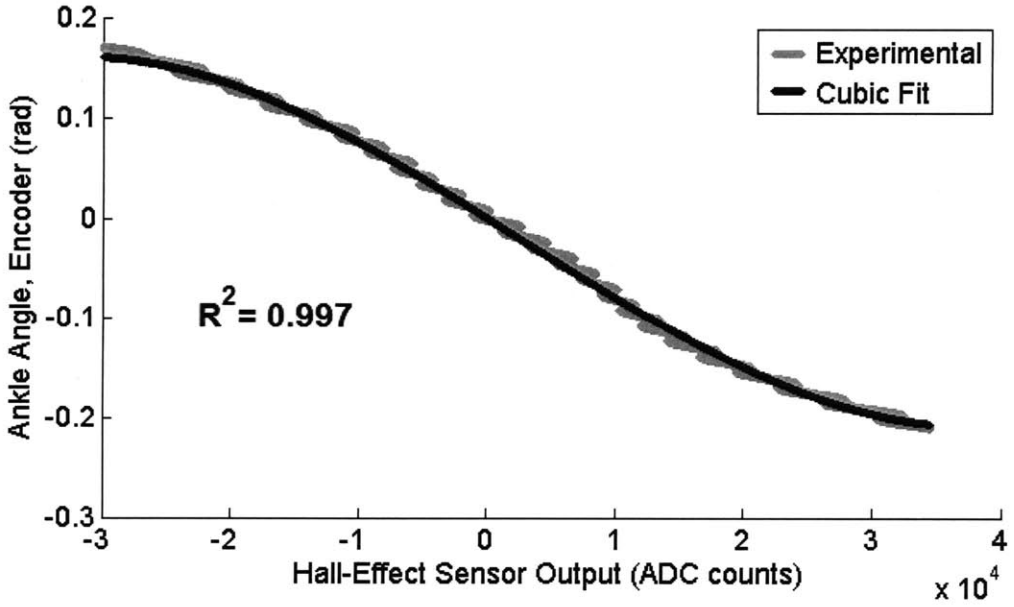

Figure 4-8: Hall-effect sensor calibration

A third-order polynomial fit (see Appendix A) centered around [0,0] was used to approximate the relationship between the ankle angle as measured from the motor encoder and the Hall-effect sensor output.

4.4. Parallel Spring Selection

As with the design of most mechanical systems, the minimization of weight is high in priority when designing a prosthesis. The incorporation of a spring in parallel with the actuator is an effective way to reduce the required motor size and simultaneously lower power consumption. In this section, the parallel spring effect on ankle behavior is analyzed.

The parallel spring reduces the required actuator torque as follows:

$$T_{act} = \begin{cases} T_{ank} - K_{parallel}\theta & \theta > 0 \\ T_{ank} & \theta \leq 0 \end{cases} \tag{4.6}$$

where T_{act} is the ankle torque due to the actuator, and K_{parallel} is the stiffness of the parallel spring. The required actuator torque T_{act} is clearly reduced for high values of K_{parallel} and θ for a given ankle torque T_{ank}. Since the largest ankle torques in human walking occur for $\theta > 0$, this reduced torque requirement allows for the selection of a smaller, lighter motor.

The goal of the parallel spring selection is to maximize the ankle torque provided by the parallel spring during the gait cycle without having the spring provide too much torque at any point in time. Therefore, the parallel spring selection was performed by estimating the spring-like component of the biological ankle torque, and therefore the ideal stiffness for human walking. The most direct way to find the parallel spring component is to divide the biological ankle torque by the biological ankle angle. The resulting trajectory is the ankle stiffness trajectory over the course of a gait cycle. This stiffness profile for $\theta > 0$ can be seen in Figure 4-9 (using the biological ankle trajectory from Section 3.4.2) for a moderate walking speed of 1.28 m/s. Dorsiflexion torques were ignored, since only the unidirectional contribution of the parallel spring was of interest (for providing plantar flexion torque). A second method of selecting the parallel spring is shown in Figure 4-10, where a simulation of parallel spring torque contribution was performed for varying parallel spring stiffness values given the moderate-speed biological ankle trajectory from Section 3.4.2.

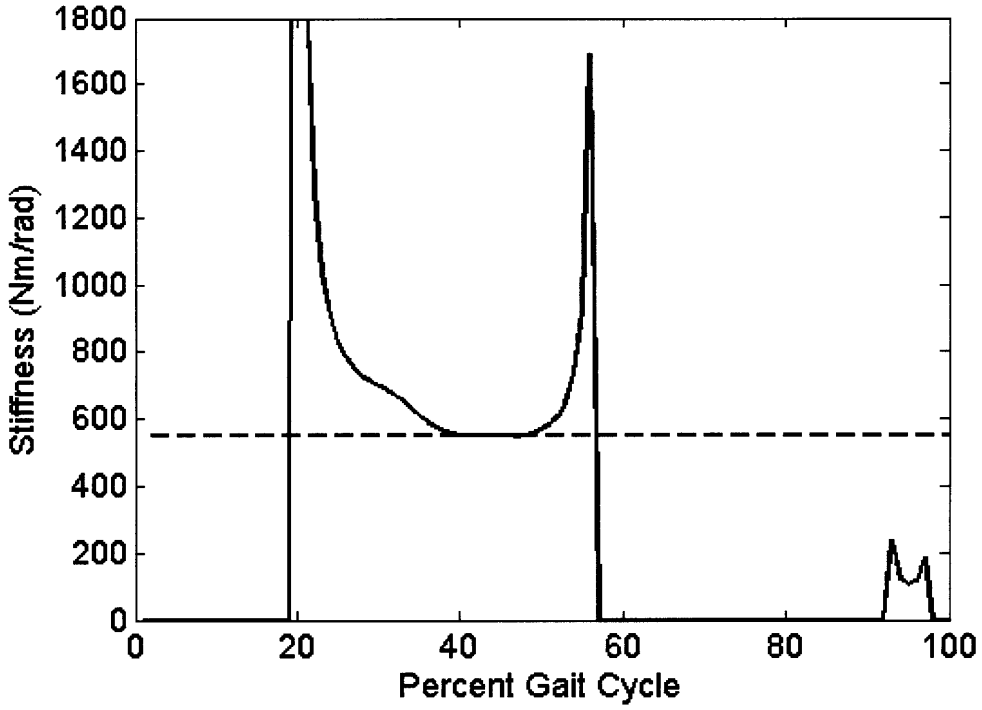

Figure 4-9: Biological ankle spring stiffness profile and minimum stiffness (dotted line) during the stance phase. (Biologic data from source described in Chapter 3)

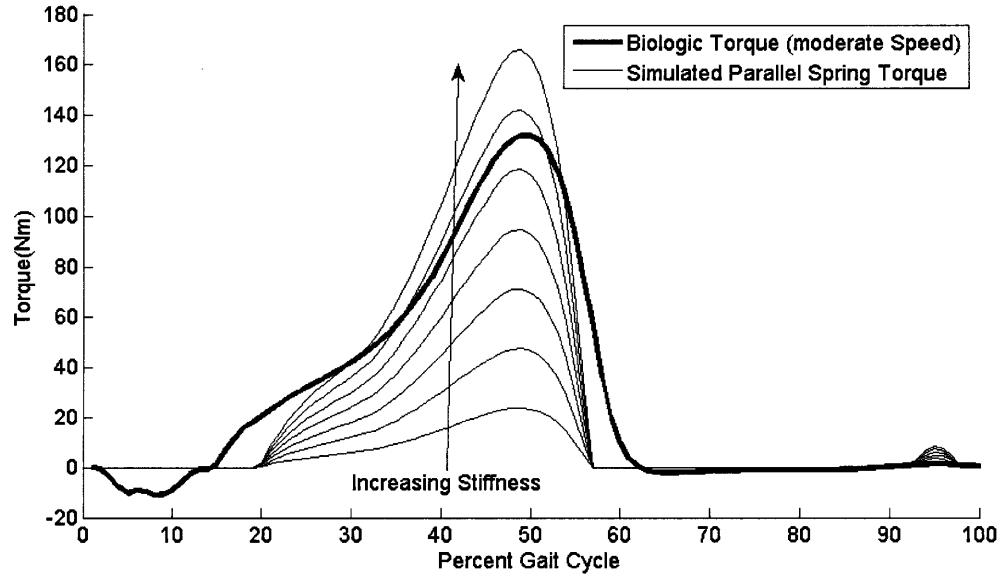

Figure 4-10: Parallel spring contribution to joint torque given the moderate-speed biological ankle angle profile described in Chapter 3.

For minimum actuator energy consumption, the parallel spring with a single stiffness would account for the biological ankle torque profile over the course of a gait cycle. If

this virtual-spring behavior was always exhibited by the human ankle, the stiffness profile in Figure 4-9 would be a straight, horizontal line, and the actuator would not be necessary if the proper spring stiffness was selected. However, since the ankle is usually responsible for generating considerable positive net work at moderate to fast walking speeds [6], the motor must modulate the apparent parallel spring stiffness to achieve the desired torque profile.

It is not desirable to allow the parallel spring torque to exceed the desired ankle torque, since the motor would have to work against the spring to reduce the effective spring stiffness, resulting in spring cancellation. Therefore, the parallel spring stiffness should be selected such that its contribution to the ankle torque during walking never exceeds the desired torque. The lowest positive stiffness shown in the stance phase (0 to ~60% GC) of (Figure 4-9 of 550 N·m/rad would be the maximum stiffness to satisfy this requirement. In this study, a slightly smaller stiffness of 500 N·m/rad was selected to allow for changes in walking behavior from the moderate biologic walking speed without requiring spring cancellation. The large peaks shown in Figure 4-9 are due to the very small angles during those parts of the gait cycle. The peaks are not of consequence, since only the local minimum of the ankle stiffness profile is of interest.

4.5. Steady State Performance Analysis

When evaluating the torque-generation ability of a prosthesis, it is also necessary to characterize the maximum performance of the selected motor and transmission in steady-state. This characterization is required to ensure that the motor does not saturate while attempting to produce the desired torque and velocity trajectories [1]. According to [1], the prosthesis must be able to achieve a force bandwidth of at least 3.5 Hz to provide sufficient performance during level-ground walking. The analysis in this thesis focused only on the motor and ideal, linear transmission. Therefore, other torque sources, such as friction and the parallel spring were neglected. In addition, the motor was considered to be directly connected to the ankle joint through the transmission, as if the series spring was removed and replaced with a rigid member.

DC Electric motors typically have a fairly linear maximum torque-speed relationship defined by [1]:

$$T_m \leq T_m^{\max} - \omega\left(\frac{T_m^{\max}}{\omega^{\max}}\right) \tag{4.7}$$

where T_m^{max} is the zero-velocity motor torque at the operating voltage, ω^{max} is the no-load speed of the motor at the operating voltage, ω is the motor velocity, and T_m is the motor torque.

Since the torque at the ankle joint was of interest, the effect of the transmission on the motor was taken into account. As a result, it was possible to evaluate the maximum performance at the ankle joint. Assuming a constant transmission ratio R, (and the lack of the series spring) the following relationships applied: [1]

$$T_{ank} = T_m R \tag{4.8}$$

and

$$\dot{\theta} = \frac{\omega}{R}. \tag{4.9}$$

The bound described by Eqn. (4.7) then resulted in a range of achievable ankle torques defined by: [1]

$$T_{ank} \leq R T_m^{\max} - R^2 \dot{\theta} \frac{T_m^{\max}}{\omega^{\max}} \tag{4.10}$$

where $\dot{\theta}$ is the ankle angular velocity, and T_{ank} is the ankle torque. Furthermore, defining ankle power as $P_{ank} = T_{ank}\dot{\theta}$, a power-velocity relationship was derived for the ankle power capability of the system (Eqn. (4.11)).

$$P_{ank} \leq R T_m^{\max} \dot{\theta} - R^2 \dot{\theta}^2 \frac{T_m^{\max}}{\omega^{\max}} \tag{4.11}$$

Eqns. (4.10) and (4.11) describe the maximum limits of the motor-transmission actuator. To ensure that the actuator can track the desired torque profiles, the torque-velocity and power-velocity curves described by the desired ankle behavior (From Section 3.4.2) must remain within the bounds described by these equations.

Assuming a fixed transmission ratio is of 200, Eqn. (4.10) resulted in the bounds shown in Figure 4-11, while Eqn. (4.11) produced the bounds in Figure 4-12. The corresponding torque-velocity and power-velocity curves for the moderate-speed biological ankle trajectories (from Section 3.4.2) are shown in their respective figures for comparison. Note that in Figure 4-12 multiple loops arise in power-velocity space. The largest loop corresponds to the powered push-off during PP. The smaller loops near the origin correspond to the remainder of the gait cycle. Since only the maximum power is of interest for a given velocity, the small loops were ignored.

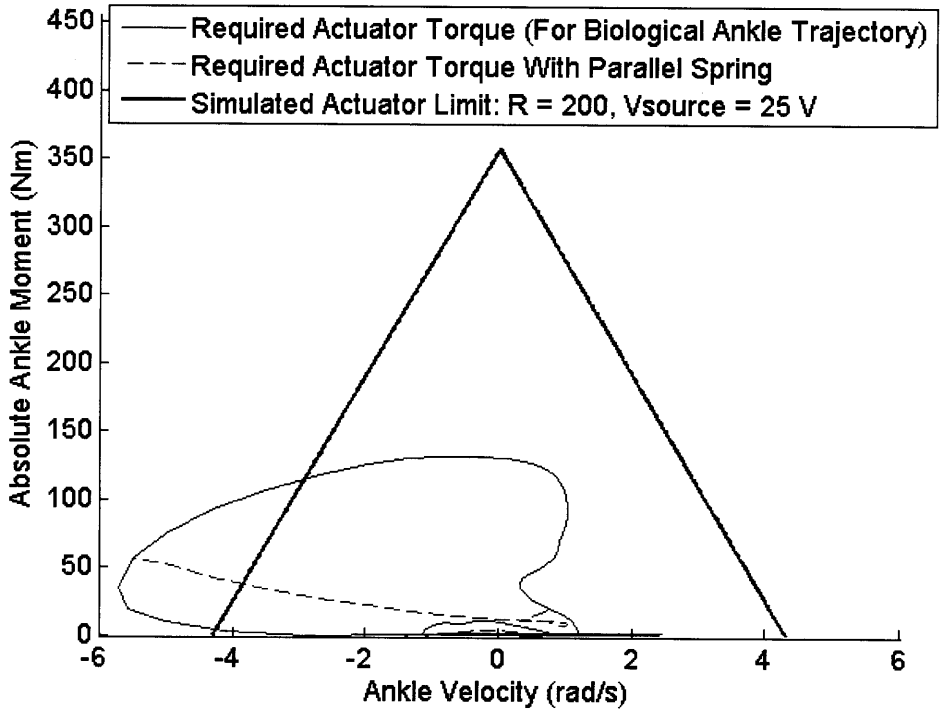

Figure 4-11: Ankle torque-velocity limits for (moderate walking speed)

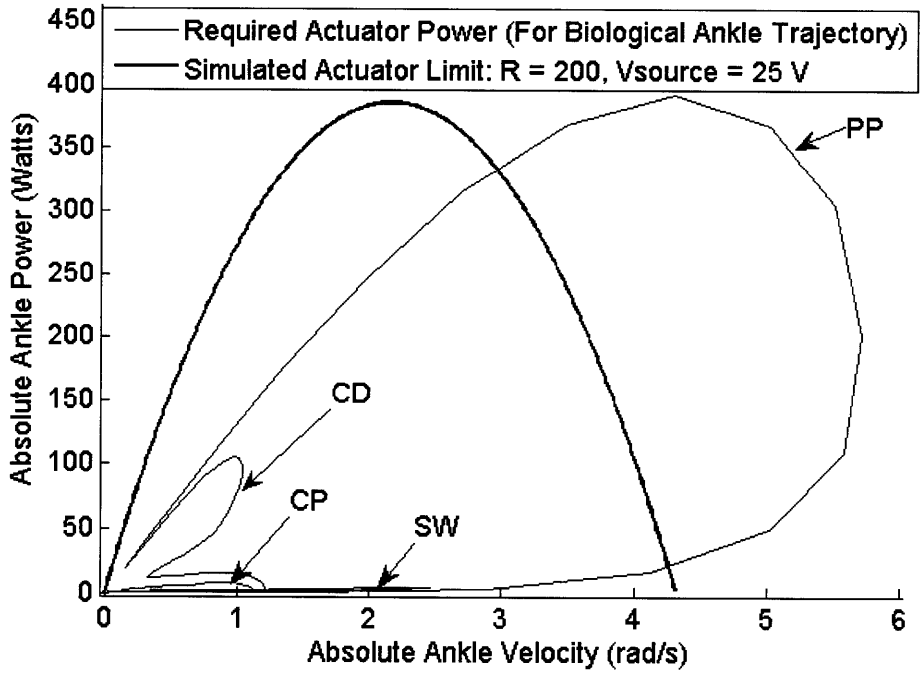

Figure 4-12: Power-velocity limits (moderate walking speed)

It is clear from the above simulation that motor saturation is expected to occur if the prosthesis controller were to command the torque and velocity profile of the biological ankle. The presence of the parallel spring can reduce the torque load on the motor as described in Section 4.4. However, as shown in Figure 4-11, the spring cannot reduce the maximum motor velocity, and hence would not prevent motor saturation in this case.

4.6. Dynamic Performance Analysis

In addition to the analysis of the steady-state behavior described in Section 4.4, it is important to examine the dynamic behavior of the prosthesis. The large transmission ratio allows for the application of extremely high steady-state torque values at the ankle joint, but limits the peak ankle acceleration. To assess the dynamic abilities of the system, the peak acceleration was found as a function of transmission ratio and maximum possible frequency oscillation at the largest required torque level (large force bandwidth) [15].

4.6.1. Transmission Effect on Acceleration

In this section, the ability of the prosthesis to propel the wearer up and forward during powered plantar flexion, as described by [1], is evaluated. For this analysis, it was assumed that the ankle joint was set at the neutral position ($\theta = 0$) and that only the toe of the prosthesis was touching the ground (Figure 4-13). It was therefore possible to model the prosthesis-amputee system as a mass, M, (representing the amputee) at the top of the shank, driven along the axis of the shank by the actuator acting on a lever arm, l. The distance l was defined as the distance from the toe of the foot to the ankle joint, estimated for this prosthesis to be 19 cm. The ankle joint was assumed to be driven by the actuator model from Section 4.2. Once again, the parallel spring, friction, and series spring were ignored for this analysis. Under these conditions, according to [1], the theoretical acceleration of the ankle joint was defined by Eqn. (4.12).

$$\ddot{\theta} = \frac{T_m R}{M l^2 + I_m R^2} \tag{4.12}$$

Also from [1], the optimal transmission to maximize acceleration for a given load M was:

$$R_{opt} = \sqrt{\frac{M l^2}{I_m}} . \tag{4.13}$$

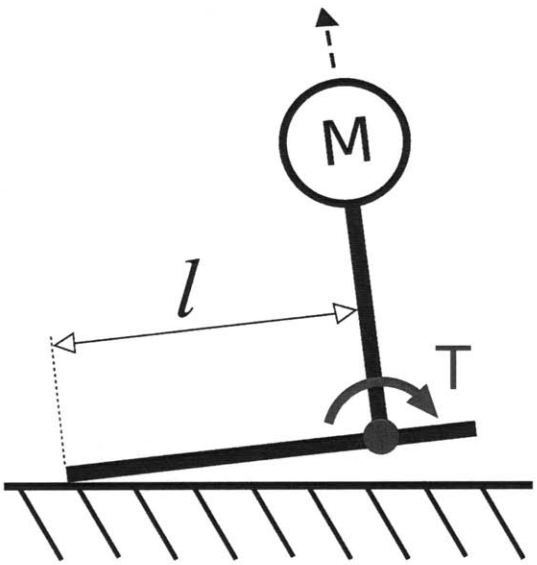

Figure 4-13: Model of the prosthesis driving a fixed load as an evaluation of the prosthesis acceleration capabilities. The torque shown is applied by the ankle on the shank.

Since the maximum performance of the actuator was of interest, the maximum available torque of the motor, T_m^{max} in place of T_m in Eqn. (4.13) was used. This maximum motor torque of a DC motor can typically only be achieved at zero motor velocity. This zero-velocity condition was assumed since only the maximum instantaneous acceleration was being evaluated. Figure 4-14 shows the acceleration in Eqn. (4.12) using $T_m=T_m^{max}$ as M is varied.

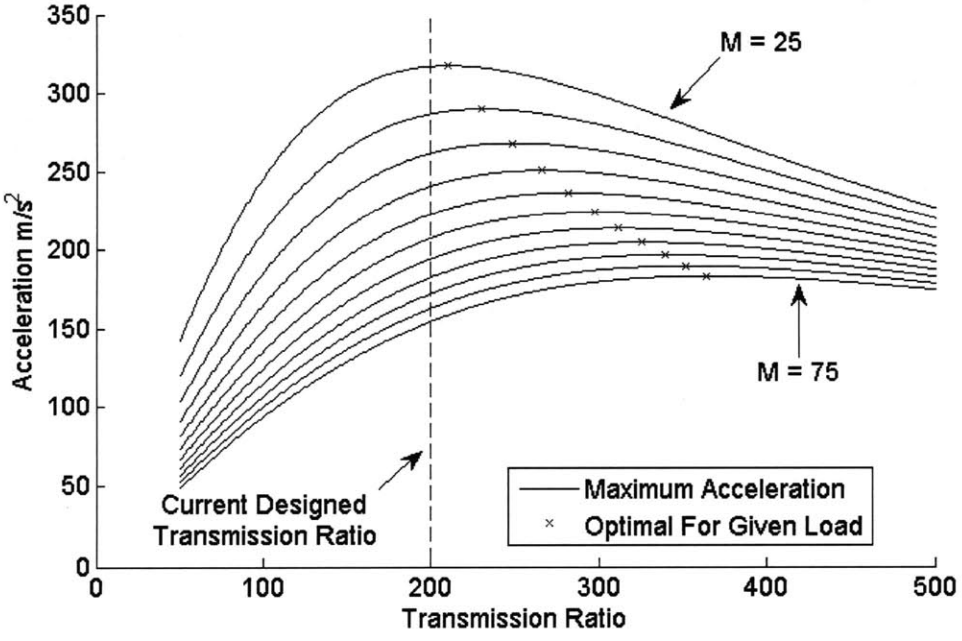

Figure 4-14: Transmission, load effect on output acceleration

The designed transmission ratio of the prosthesis was considerably lower than the optimal for a typical subject mass of 75 kg. However, as discussed in Section 4.5, the transmission ratio was already high enough to cause the motor to saturate during normal walking. Therefore, the selected transmission ratio resulted in a tradeoff between motor saturation and maximum instantaneous acceleration.

4.6.2. Large force bandwidth analysis

Although the general system model used in this thesis neglects motor saturation effects, it is wise to consider the worst-case scenario when the motor is operating close to its saturation limit. In this regime, a decrease in force bandwidth occurs. This reduced force bandwidth can be modeled by including motor saturation effects in the system model and assuming input motor torques close to the motor saturation limit. One tool for evaluating the resulting actuator performance is called the large-force bandwidth. The large force bandwidth is defined as the frequency range in which the system can produce an oscillatory torque output at a particular amplitude [1], given the maximum input motor torque amplitude, T_m^{max}. To model the torque-velocity constraint along the edge of the motor's operating range, the motor was modeled as a linear damping term [1]

$$B_{sat} = \frac{T^{sat}}{\dot{\theta}^{sat}} \tag{4.14}$$

in parallel with an ideal torque source. Here, $T^{sat} = RT_m^{max}$ and $\dot{\theta}^{sat} = \omega^{max} / R$, where T^{sat} = 1.79 N·m/A, and $\dot{\theta}^{sat}$ = 900 rad/s at the operating voltage of 25 V. The maximum performance of the actuator in frequency space was determined by including this additional damping term into the system model from Eqn. (4.21):

$$\frac{T_{ank}^{max}}{T_e} = \frac{K_s}{I_e s^2 + (B_e + B_{sat})s + K_s} \tag{4.15}$$

where the values for I_e, B_e, and K_s were obtained in Section 4.7.3, T_e is the effective motor torque through the transmission and T_{ank}^{max} is the torque output of the system.

The magnitude plot for the frequency response of Eqn. (4.15) is shown in Figure 4-15. The value of the large force bandwidth depends on the amplitude of interest, so two torque amplitudes were selected for comparison to the output of Eqn. (4.15). The first torque amplitude of interest was the prosthesis actuator torque needed to provide the maximum biological ankle torque from the human walking data discussed in Section 3.4.2. The second torque amplitude was this same amplitude including the reduction in torque provided by the prosthesis parallel spring, as described by Eqn. (4.6). Both torque values were normalized by T^{sat}. These normalized torque values were then superimposed on the plot in Figure 4-15. It is clear that, in Figure 4-15, the large force bandwidth for tracking the biologic torque profile is lower than the required biological frequency of 3.5 Hz. However, since the parallel spring greatly reduces the load required by the actuator

according to Eqn. (4.6), the large-force bandwidth for the reduced torque value is sufficiently increased as a result of the addition of the parallel spring.

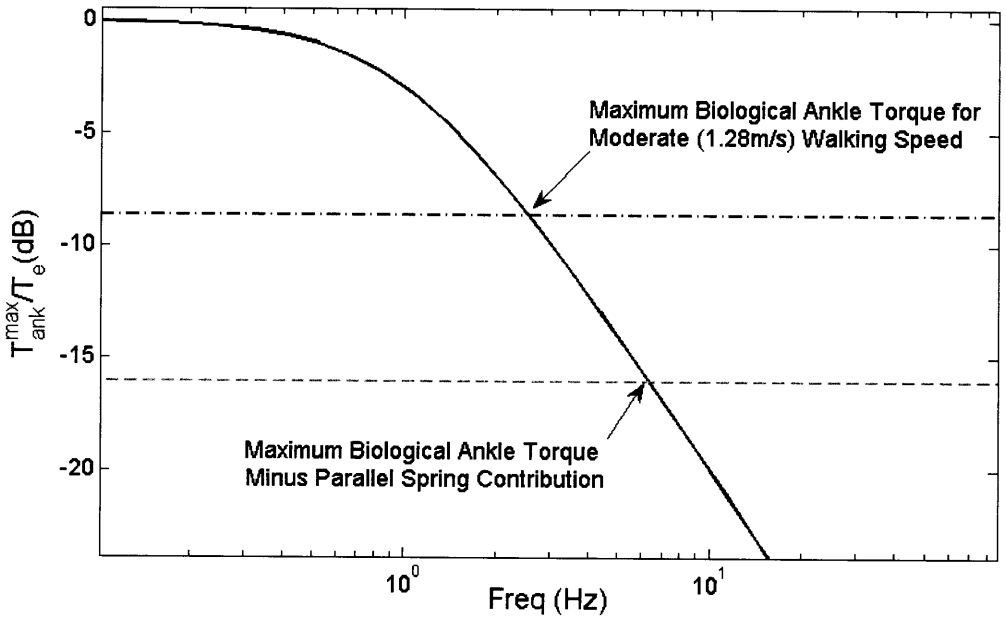

Figure 4-15: Large force bandwidth

4.7. System Characterization

To fully describe the physical system, it was necessary to find the parameter values in the system model (described in Section 4.2). To accomplish this, a system characterization procedure was performed, as discussed in the following sections.

4.7.1. Model Parameter Estimates

Using the total transmission R = 200 and the motor inertia I_m = 33.3gcm^2, Eqn. (4.1) resulted in an equivalent inertia seen at the ankle joint of 0.1332 kg·m^2. Although the ballscrew, timing belt pulleys, and other components also contribute to the effective inertia, these were ignored since the motor inertia, seen through a transmission of the highest gear ratio, dominates.

Neither the damping of the motor nor that of the rest of the drivetrain was known to a high degree of accuracy. Therefore, B_e was evaluated experimentally in Section 4.7.3. Also, although prior estimates were known for the two series spring constants, K_s was also evaluated experimentally for comparison.

4.7.2. Bench Setup

A bench setup, shown in Figure 4-16, was assembled in order to obtain experimental values for the system model by fixing both ends of the prosthesis. The goal of this set of tests was to obtain the missing parameters of the linear model and to evaluate the ability of the resulting model to characterize the physical system.

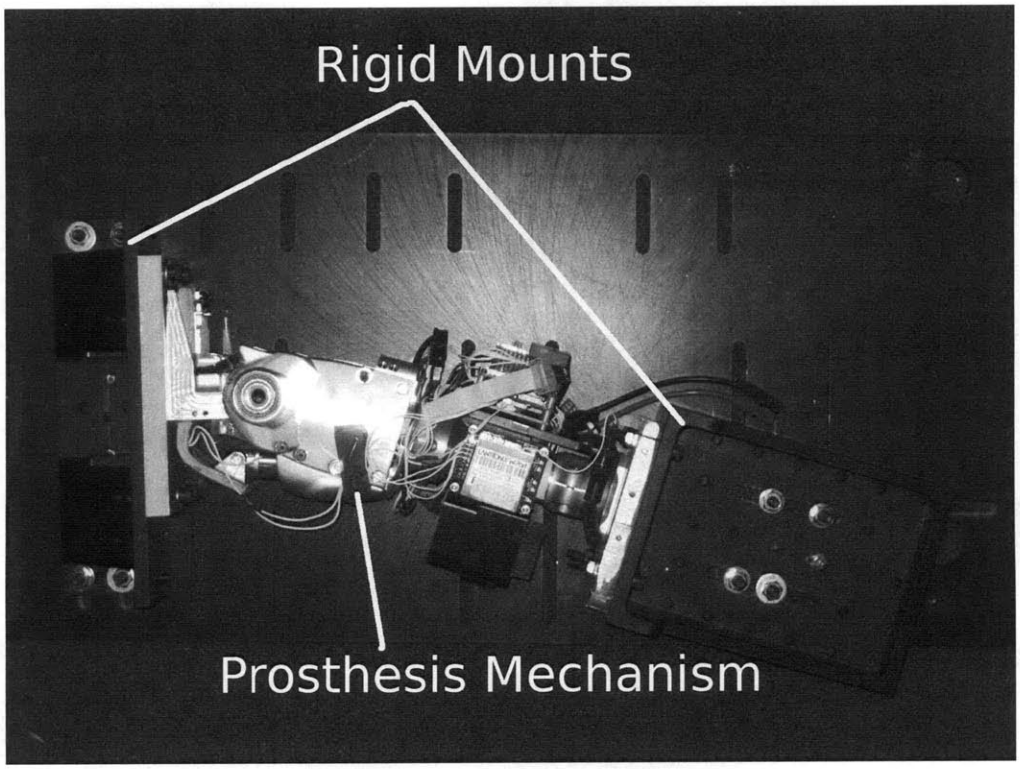

Figure 4-16: Experimental Bench Test Setup

The parallel spring was removed for the purposes of these tests, since the intent was to model the actuator only. The carbon leaf-spring foot was also removed for this reason. The base plate of the prosthesis was then screwed directly into an Aluminum plate, which, in turn, was anchored to a large platform. The platform was clamped to a large table in order to minimize external dynamics from the bench setup.

A 112 mm-long aluminum tube was rigidly attached to the prosthetic pyramid at the top of the ankle. The free-end of this tube was fixed to the platform. This aluminum tube was included in the tests both to provide a mount for the ankle electronics and to simulate the conditions of the clinical trials, since the same-length tube would be used in the clinical trials.

A chirp command in current (Figure 4-17) was applied to the motor starting at 0.5 Hz and increasing to 30 Hz in discrete intervals while measuring the ankle torque using the series spring strain gauge. Discrete frequency intervals were chosen to maximize the exhibition of steady-state behavior over frequency. Zero torque was commanded for 0.5 seconds between each pair of consecutive frequencies to provide a clear distinction

between the different frequencies. To limit the forces exerted on the system during these tests, the commanded current was reduced close to the resonant frequency.

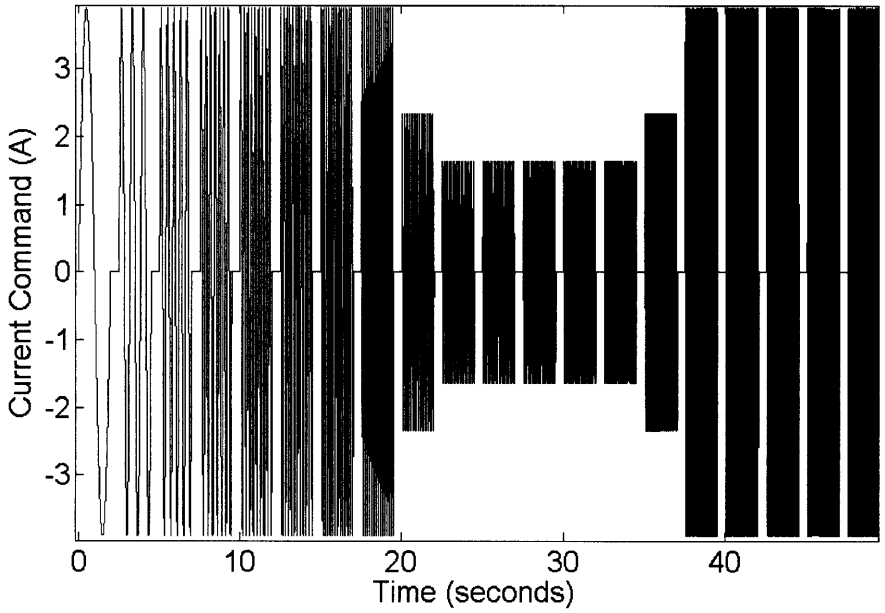

Figure 4-17: Discrete-frequency chirp signal with current-command reduction near the resonance.

4.7.3. System Identification

The Matlab function *tfestimate* was used to estimate the frequency-domain relationship between the desired ankle torque and the measured ankle torque as measured by the series spring strain gauge for the 4-Amp amplitude discrete chirp test. The inputs to this function were the commanded chirp torque and the measured ankle torque from the series spring strain gauge. The commanded chirp torque was calculated from the motor current command using Eqn (4.4).

The experimental frequency response curve can be seen in Figure 4-18. It is important to note that the *tfestimate* function also returns a covariance curve over frequency, which indicates the accuracy of the estimation. The frequency response was analyzed for only the frequency range at which the covariance was close to 1 (> ~0.8).

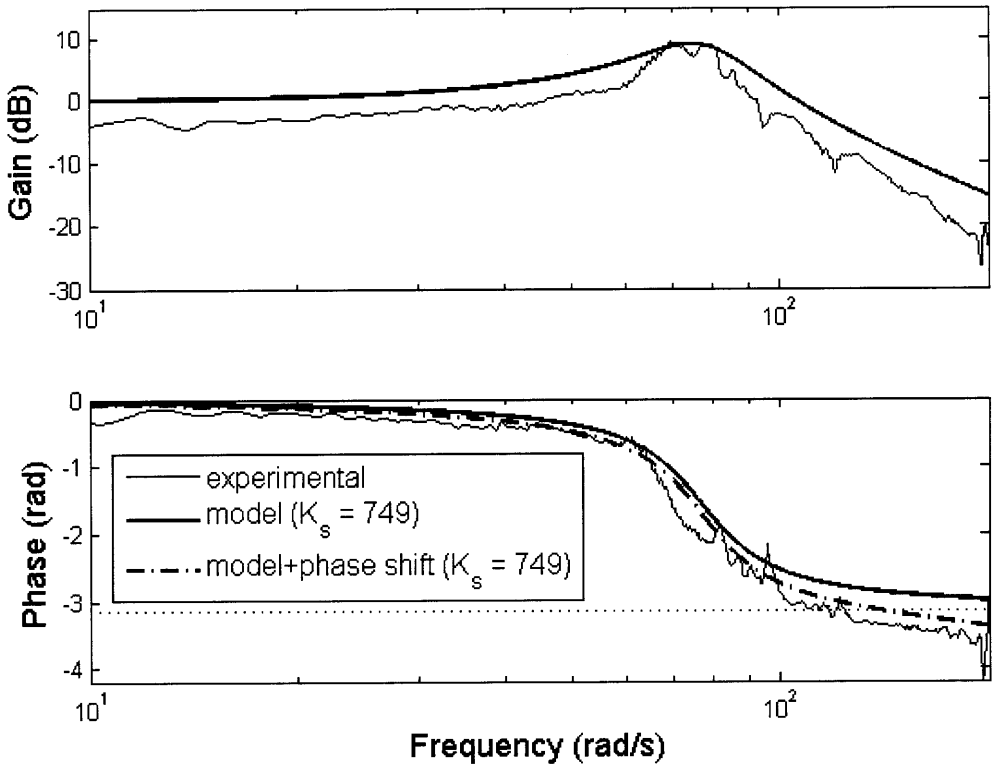

Figure 4-18: Frequency response: simulation vs. experimental

A general second-order transfer function, (Eqn. (4.16)), where s is the Laplace variable, was fit to the measured frequency-response curve.

$$\frac{T_{ank}}{T_{comm}} = \frac{\omega_n^2}{s^2 + 2\zeta\omega_n s + \omega_n^2} \tag{4.16}$$

The location and approximate height of the resonant peak were used to obtain estimates for the natural frequency and damping parameters respectively. The damping ratio was estimated using the relationship [11]:

$$M_P = \frac{1}{2\zeta\sqrt{1-\zeta^2}} \tag{4.17}$$

where M_P is the resonant peak height, (as a gain factor), above the steady-state gain of 0. The result of this fit produced estimates of the resonant peak frequency $\omega_P = 75$ rad/s and damping ratio $\zeta = 0.18$. An undamped natural frequency $\omega_n = 77.6$ rad/s was found by the relation [11]:

$$\omega_n = \frac{\omega_P}{\sqrt{1-2\zeta^2}}. \tag{4.18}$$

The effective series spring stiffness was estimated as K_s = 749 using Eqn. (4.19), which is derived by equating Eqns. (4.3) and (4.16).

$$K_S = \omega_n{}^2 I_e \tag{4.19}$$

This value of K_s does not accurately represent any one series spring stiffness, but represents a combination of the two stiffness values of the series spring (1200 and 533 N·m/rad). However, since the plantar flexion torque production was of primary interest, only the plantar flexion direction of the series spring was considered. Therefore, the plantar flexion stiffness of K_s = 533 N·m/rad was used in the model. As a result, the system characterization analysis only applied to the application of positive joint torque. The damping coefficient, however, was obtained experimentally using Eqn. (4.20), (again by equating Eqns. (4.3) and (4.16)) since the physical damping value was independent of the spring stiffness value. Using the value of I_e = 0.1332 kg·m^2 from Section 4.7.1, this calculation resulted in B_e = 3.7 N·m·s/rad.

$$B_e = 2\zeta\omega_n I_e \tag{4.20}$$

Using the values of I_e, B_e, and K_s described above, the frequency response of the modeled system can be seen in Figure 4-18.

In addition to the mechanical effects described in Section 4.2, a time-delay was expected due to sampling and computational effects of the onboard microcontroller. This time-delay was manifested in the frequency domain as a phase shift beyond that of the second-order system described by Eqn. (4.16). This additional phase shift of the physical system as compared to the model without a delay can be seen in Figure 4-18. The phase shift was incorporated into the system model using the factor $\exp(-t_d s)$ where t_d, the time delay in seconds, was set to 0.002 seconds, based upon estimates of the computational delays from the microcontroller. The resulting modeled phase lag can be seen in Figure 4-18. Using this phase shift factor, a slightly more accurate transfer function, as shown in Eqn. (4.21) was obtained. The model parameters are summarized in Table 4-2.

$$\frac{T_{ank}}{T_{comm}} = \frac{e^{-t_d s} K_s}{I_e s^2 + B_e s + K_s} \tag{4.21}$$

Table 4-2: Summary of model parameters

I_e (kg·m^2)	B_e (N·m·s/rad)	K_s (N·m/rad)	t_d (s)
0.1332	3.7	533	0.002

As shown in Figure 4-18, the gain of the experimental frequency response curve is significantly higher than that of the model for frequencies above and below the resonance. This apparent drop in magnitude of the physical system can be attributed to un-modeled friction. Also, since the series spring strain gauge was only calibrated in one direction, the measured torque in other direction (dorsiflexion torque) may not have been accurate. This potential asymmetry may also have resulted in an apparent gain.

4.7.4. Step Response Validation

In addition to running through the frequency band, the step-response of the system was recorded at varying step magnitudes. These step-response tests are useful in that, in contrast with the frequency response analysis, which describes the steady-state behavior of the system, the step response shows how the system responds to transients. Figure 4-19 shows the experimental step response of the system for varying step commands, as compared to the model from Eqn. (4.21).

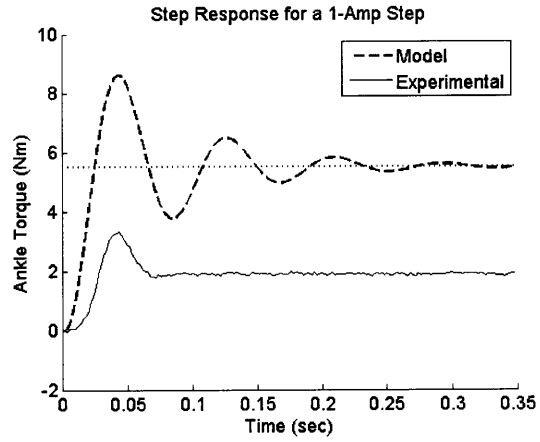

(a)

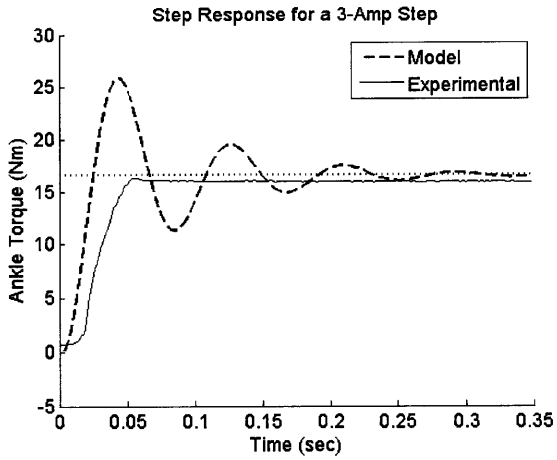

(b)

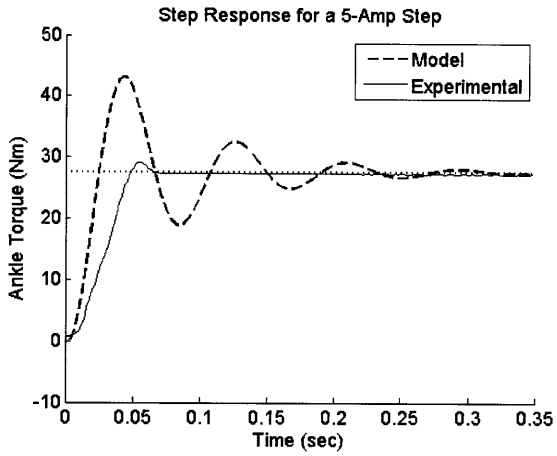

(c)

Figure 4-19: Open-loop step response showing representative experimental step trials

It is clear from Figure 4-19 that there is a significant discrepancy between the model and the experimental results. Given the relatively fast rise time, little overshoot, and no oscillations of the experimental step-response, it is likely that the discrepancy is primarily caused by coulomb friction in the drive train. This frictional effect is most apparent in the steady-state behavior of the model for the 1-amp step, where the static coulomb friction dominates over the relatively small drive train forces.

4.8. Discussion

From Section 4.7.3, it has been shown that the physical system can be generally described using a simple linear model with a linear phase shift. The results of the system frequency characterization tests indicate a second-order system with a resonance. However, it is clear from the step response plots that there exists a considerable amount of nonlinear friction in the drivetrain. The existence of this friction makes feedback control that much more important if the desired ankle torques are to be enforced. However, the nonlinear nature of coulomb friction limits the effectiveness of classical control methods.

According to Section 4.5, if the series spring is neglected, the motor is expected to saturate if the ankle torque and angle profiles match those of the biologic data. Furthermore, the presence of the parallel spring is not sufficient to solve the problem. However, since the requested torque from the neuromuscular model is a function of ankle angle, it is possible that a subject wearing the prosthesis could select ankle angle trajectories that would lead to ankle torques within the capabilities of the prosthesis. In addition, the presence of the series spring, although harmful to the system force bandwidth, ([15]), allows the actuator to provide considerably higher instantaneous power than would otherwise be possible [12]. Therefore, it is possible that the presence of the series spring can help compensate for the torque-velocity saturation limits of the motor-transmission mechanism.

5. Control Design

For the proper evaluation of the reflex muscle model detailed in Chapter 3, it was necessary to ensure that the mechanical system would track the desired trajectory as closely as possible. It became clear, after the initial open-loop step-response trials, that the inherent friction in the drive train seen in Figure 4-19 would likely prevent the precise control of joint torques without some form of error compensation. The need for disturbance rejection also motivated a feedback torque controller. Therefore, a control system was designed that incorporated a standard feedback controller, feedforward corrections, and finally, a specialized torque-feedback term to correct for some frictional effects.

5.1. Overall Control System

The overall control architecture is outlined in Figure 5-1. The neuromuscular model and impedance controller, as described in Chapter 3, was used to provide a desired torque command to the force controller. The purpose of the control system is to convert desired torque from the neuromuscular model and impedance controller, τ_d, to produce a torque-command to the prosthesis, τ_c. The torque command is converted into an appropriate torque by the prosthesis motor controller. The control system comprises a lead compensator as part of a feedback torque controller, a feedforward gain K_{ff}, and positive torque-feedback term. Each of these subsystems is described in detail in the following sections.

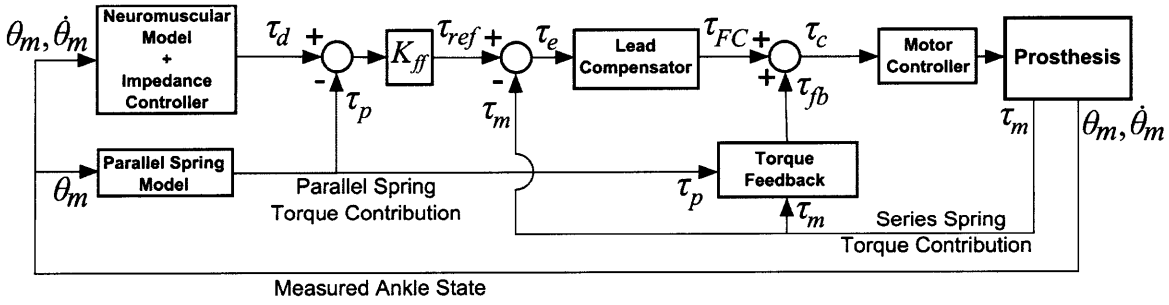

Figure 5-1: Overall control architecture

5.2. Feedforward Terms:

The torque used for the feedback controller was measured at the series spring and therefore did not include the torque from to the parallel spring. Therefore, for the purposes of control, the parallel spring torque estimate (as calculated using Eqn. (4.6)) was subtracted from the neuromuscular model's desired torque, τ_d, using the measured ankle angle, θ_m, as determined from the prosthesis Hall-effect sensor.

A feedforward gain, K_{ff}, was then applied to the resulting actuator-desired torque signal to obtain τ_{ref}, the reference torque for the feedback controller. The value of K_{ff} was selected using the inverse of the steady-state gain from the closed-loop step-response test in Figure 5-3. As a result, the ultimate effect of K_{ff} was to decrease the steady-state error of the controller without the use of an integrator or lag compensator. Although feedforward gains like this one can decrease the steady-state error of the closed-loop system without sacrificing performance, they cannot improve the disturbance rejection of the system. Section 5.3 discusses why this term was chosen instead of the additional lag compensator.

5.3. Feedback Controller

The feedback controller included a torque feedback loop, using the series spring torque measurement, to enforce the desired output torque. The compensator was implemented as follows:

$$\tau_{FC} = (\tau_{ref} - \tau_m)C(s) = \tau_e C(s) \tag{5.1}$$

where τ_{FC} is the feedback controller torque output, τ_m is the measured actuator torque as obtained from the series spring strain gauge, and $C(s)$ is the compensator transfer function. τ_e is the torque error as seen in Figure 5-1.

The feedback controller was programmed to take effect only during the LS state, when exclusively positive torque is applied. This restriction was implemented because the system analysis in Section 4.7, and consequently, the control design, only applied for positive prosthesis torque. For this reason, $C(s)$ (and associated K_{ff}) were only enabled during the LS state, where only plantar flexion torque was developed. Open-loop torque control (with $K_{ff} = 1$) was used to command ankle torque for the remainder of the gait cycle.

The compensator was tuned for the system model in Eqn. (4.21) as the plant. It was found that the addition of an integrator or lag compensator hurt the mid-range performance too much to be worth the advantage of the zero steady-state error for a step input. Therefore, a single lead compensator of the form

$$C(s) = K_L \frac{\alpha \mathrm{T}s + 1}{\mathrm{T}s + 1} \tag{5.2}$$

was selected as a compensator, and K_{ff} was used to reduce the steady-state error. In Eqn.(5.2), α is the lead ratio, T is a time-constant, and K_L is the compensator gain. A cross-over frequency of 150 rad/s was chosen to maximize bandwidth without needing to reduce phase lag by more than 0.7-0.85 radians for sufficient phase margin. (See Figure 4-18 for a Bode plot of the uncompensated system.) The zero of the lead compensator was placed at 75 rad/s and α was made large enough such that the cross-over frequency was closer to the zero than to the pole. As a result of this zero and pole placement, a

larger compensator gain was possible than if the cross-over frequency had been more centered between the pole and zero. This increased gain helped to minimize the steady-state error introduced by the feedback loop. A large value of α was chosen to obtain a phase margin of at least 45 degrees. The compensator gain, K_L was then tuned to provide the desired closed-loop bandwidth.

Un-modeled effects, such as additional phase lag and possibly effects from the nonlinear series spring resulted in the need for slightly stronger stability margins than otherwise modeled. Final adjustments were therefore made using the physical system to ensure stability while maintaining the desired response. The parameters of the resulting compensator can be seen in Table 5-1. This lead compensator resulted in theoretical closed loop force bandwidth of 147 rad/s, as shown in Figure 5-2. This bandwidth is sufficient for the required 22 rad/s (3.5 Hz) force bandwidth of the prosthesis.

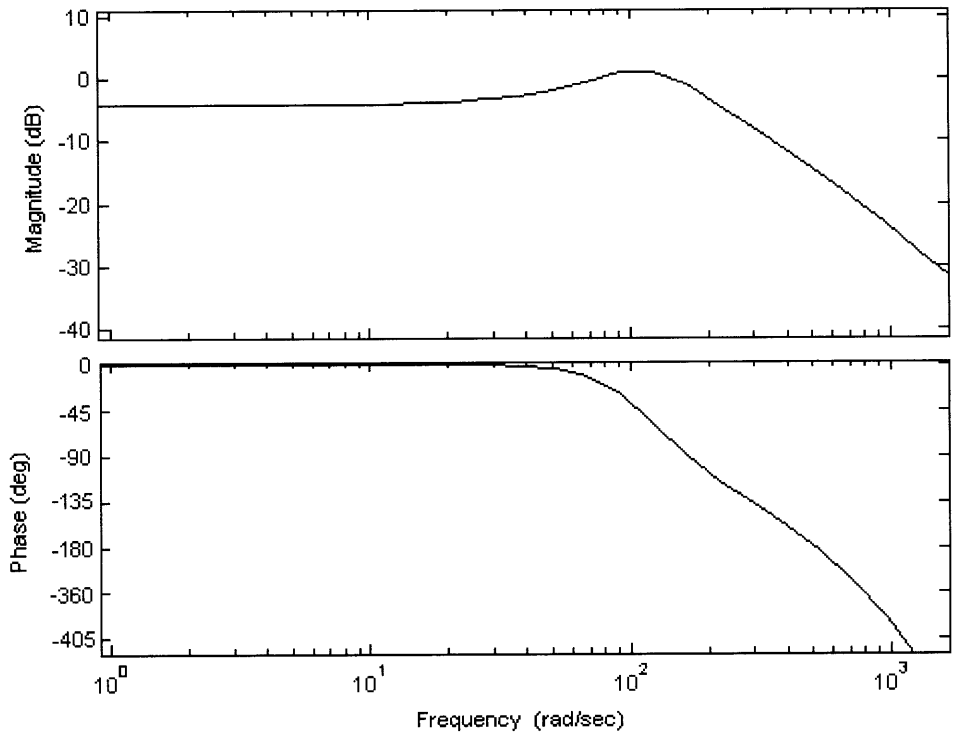

Figure 5-2: Closed-loop frequency response simulation of the compensated system

In firmware, the lead compensator was implemented as a difference equation. A bilinear transformation [3],

$$s = \frac{2}{T}\left(\frac{z-1}{z+1}\right) \tag{5.3}$$

was used as an approximate mapping of the designed compensator from the Laplace domain into the Z domain. A difference equation was then derived from the Z-domain transfer function using $\mathcal{Z}^{-1}\{z^{-1} X(z)\} = x(k-1)$ [3], where $\mathcal{Z}^{-1}$ is the inverse Z-transform

and x(k) is a function x evaluated at sample k. The C code for the compensator may be seen in Appendix B.

5.4. Torque Feedback Term

It was found in early clinical trials that despite the torque compensation described in Sections 5.2 and 5.3, the prosthesis was not generating the desired sudden increase in torque at the transition from controlled dorsiflexion to powered plantar flexion. This result was most likely due to coulomb frictional effects and binding. Therefore, it was suggested that a torque-feedback term be added to the control effort during powered plantar flexion to help overcome nonlinear frictional effects and force the desired torque profile. This torque-feedback term was programmed to activate at maximum dorsiflexion, when the ankle angular velocity initially dropped below zero during the LS state. The torque-feedback term was defined as follows:

$$\tau_{FB} = K_{FB}\left(\tau_m + \tau_p\right)^{E_{FB}} \tag{5.4}$$

where K_{FB} and E_{FB} are the torque-feedback constant and torque-feedback exponent respectively. These two constants were tuned experimentally during initial clinical tests to maximize torque tracking. The exponent was tuned to increase the torque-feedback correction term at higher angle values, such as at the beginning of PP, whereas the gain was tuned to adjust the magnitude of the torque-feedback for the remainder of PP. The final values for the torque-feedback parameters are listed in Table 5-1.

Table 5-1: Parameters for control

Parameter	Value
K_L	1.64
T	9.93 e-4 s/rad
α	13.4
K_{ff}	1.7
K_{FB}	0.24
E_{FB}	1

5.5. Torque Controller Evaluation

The step response of the compensated system was chosen as a means of evaluating the feedback controller. This method of evaluation was used for three reasons. Firstly, the step response of a system fully describes that system over all frequencies. Secondly, the steady-state response of the system can be evaluated easily, and compensated using the feedforward gain. Thirdly, the nonlinear series spring prevents a frequency-domain evaluation of the control system performance for exclusively positive torque values. This

limitation arises because both sides of the series spring contribute to the frequency response, as discussed in Chapter 4.

Initially, only the feedback controller was used, with $K_{ff} = 1$, and a step in torque of magnitude 27.6 N·m was commanded. (This torque level is comparable to an open-loop motor command of 5 Amps.) The step-response of the simulated compensated system compared to that of the physical system can be seen in Figure 5-3. The subsequent addition of the feedforward gain eliminated the steady-state error shown.

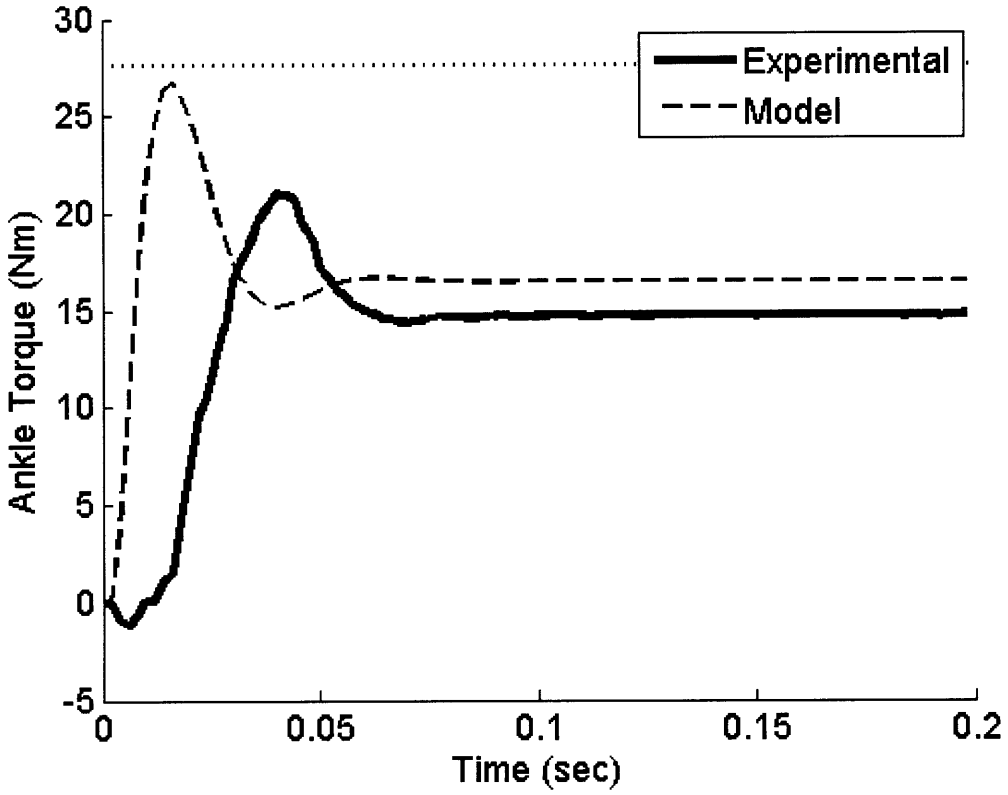

Figure 5-3: Closed-loop step response, using only the lead compensator (no feedforward gain)

Referring to Figure 5-3, the experimental steady-state error differs slightly from that of the model. In addition, the experimental torque curve shows a slower response than the simulation indicates. Un-modeled friction is likely the primary cause of these discrepancies. However, it was also found that the force controller had non-zero initial conditions when activated at the start of the commanded step. As a result, a slight negative downturn was observed at the beginning of the step response due to a short initial negative spike in torque command. This effect, although significant in Figure 5-3, was expected to be negligible in the clinical trials since the torque controller remained activated throughout the stance phase.

The controller was also tested by commanding the biologic torque profile (as described in Section 3.4.2). This biologic profile was seen as a good measure of performance, since it was thought to contain a similar frequency spectrum as the required

ankle torque profile during the clinical walking trials. The torque-feedback term was disabled for these tests to best evaluate the performance of the lead compensator and feedforward terms alone. A representative simulated gait cycle of this biologic torque profile is shown in Figure 5-4. The magnitude of the simulated torque profile was scaled down to prevent overheating of the motor, given the lack of assistance from the parallel spring.

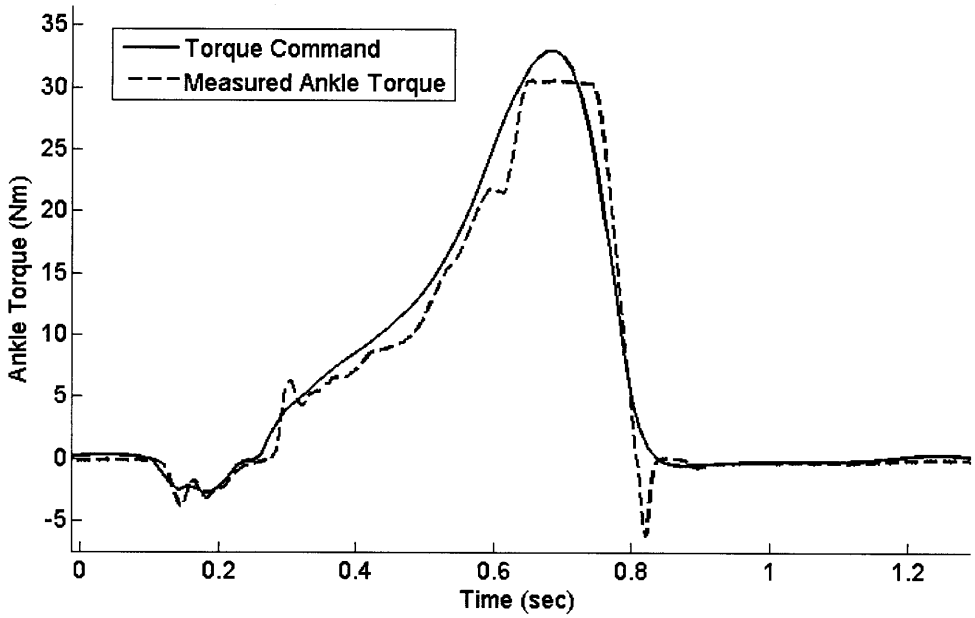

Figure 5-4: Torque following for biological torque profile

Qualitatively, the torque tracking for this controller was considered to be acceptable for most of the simulated gait cycle. Large errors were seen in certain sections of the gait cycle, however. The overshoot seen at the end of the stance phase at 0.8 seconds was consistent with that of the closed-loop step response. This overshoot may have been exacerbated by the increased stiffness of the series spring as the spring force dropped below zero. There was also a significant deviation from the torque command in the peak-torque region (~0.7 seconds). The positive torque feedback term was expected to aid in reducing the torque-error this region.

5.6. Discussion

In this chapter, a control system was developed to minimize torque tracking errors of the powered ankle-foot prosthesis. Although the feedback controller sacrificed steady-state error for bandwidth, the addition of the feedforward gain corrected for the steady-state error, as shown in Figure 5-4. The torque feedback term corrected for errors due to the frictional effects at the sudden direction change between CD and PP. The combination of these three components resulted in satisfactory torque tracking.

6. Clinical Evaluation

To evaluate the neuromuscular model described in Chapter 3, clinical trials were performed with an amputee subject for level-ground walking at slow and moderate speeds. Ramp ascent and descent walking trials were also captured. This chapter describes the clinical procedure and data processing and compares the results against the biologic data used for the muscle model optimization.

6.1. Methods

The prosthesis was placed on the right leg of a healthy, active, 75 kg bilateral trans-tibial amputee after informed consent was given. The subject was allowed time to walk on the prosthesis for natural adjustment. Both parameter sets from the optimization in Chapter 3 were programmed into the prosthesis. Either of these two parameter sets could be selected in real-time using a wireless link to the prosthesis. This same wireless link was used to record the walking data from the clinical trials.

During the level-ground walking trials, the subject was asked to walk across a 10-meter long path at the slow and moderate speeds. For each walking speed, the corresponding parameter set was enabled in the state machine and neuromuscular model, and the target walking speed was set to that of the corresponding biologic data. The subject began walking approximately 5 meters from the beginning of the pathway, and stopped walking approximately 3 meters past the end of the path. Markers on the ground were used to note the beginning and end of the 10-meter long path. A stopwatch was used to verify the average walking speed for each trial by noting when the subjects' center of mass passed over each of the markers. A total of 10 trials were captured for each walking speed. Trials with walking speeds within 5% of the target speeds were used for processing, resulting in 36 gait cycles at the moderate speed and 45 gait cycles at the slow speed.

Next, the slow-speed parameter set was enabled in the state-machine and neuromuscular model. The subject was asked to walk up an 11-degree incline at a self-selected walking speed. The subject started on level-ground approximately 2 meters from the start of the incline and stopped approximately 1 meter past the incline on a platform for 10 ramp-ascent trials. This same path was then navigated in reverse for 12 ramp-descent trials.

6.2. Data Processing

The first three and last three gait cycles of the level-ground trials were assumed to be transients, and were therefore ignored. Each of the remaining gait cycles was re-sampled

to span 1000 data points. Mean and standard-deviation trajectories were subsequently obtained from the resulting data.

For both ramp ascent and descent, the last step on the ramp was used as the representative gait cycle. Each selected gait cycle was re-sampled and averaged in the same manner as described for the level-ground trials.

The net work was calculated for each individual gait cycle by numerically integrating ankle torque over ankle angle from heel-strike to toe-off. (The swing phase was ignored for the net-work calculations.) The average net work for each walking condition was then computed from the individual gait cycle net work values.

6.3. Results

6.3.1. Torque Tracking Verification

Since the performance of the neuromuscular model was being evaluated, it was critical to ensure that the physical system was, in fact, producing the requested muscle-model joint torques within some small margin. According to Chapter 5, the torque controller was capable of tracking the expected torque profile. This torque-tracking quality for each of the walking conditions is shown in Figure 6-1 through Figure 6-4. The plots have been labeled with the same gait state markers shown in Figure 2-3 for reference.

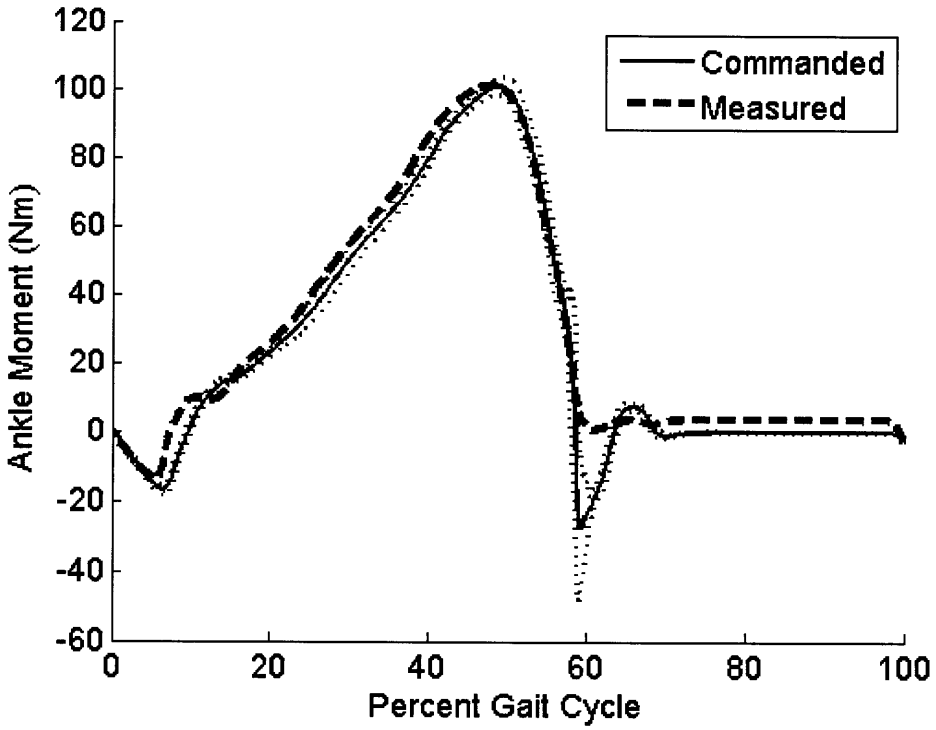

Figure 6-1: Torque tracking at moderate-speed level-ground walking.

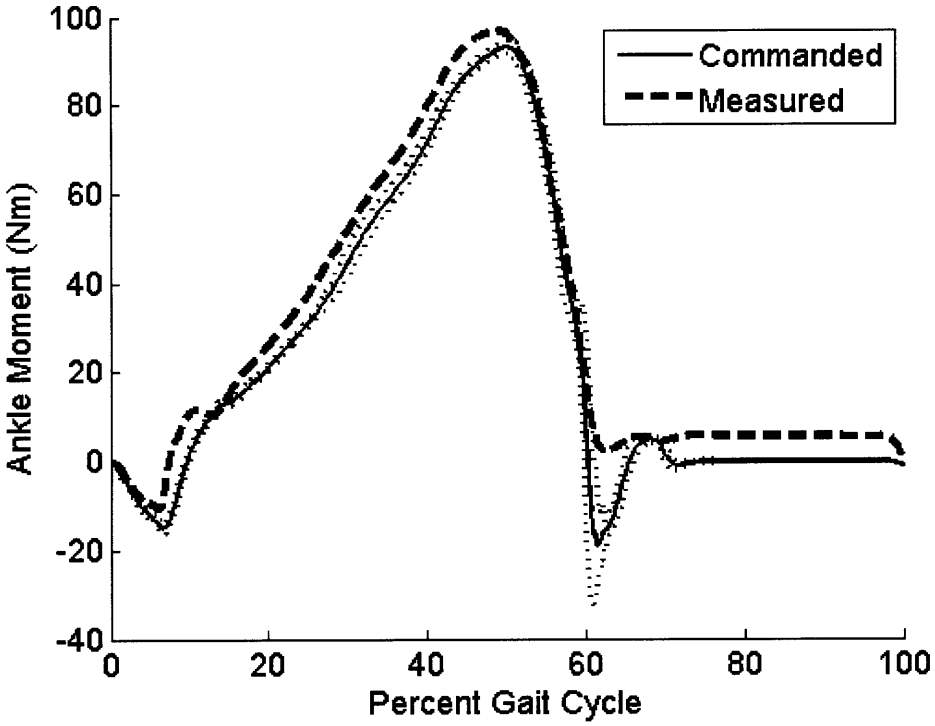

Figure 6-2: Torque tracking at slow-speed level-ground walking

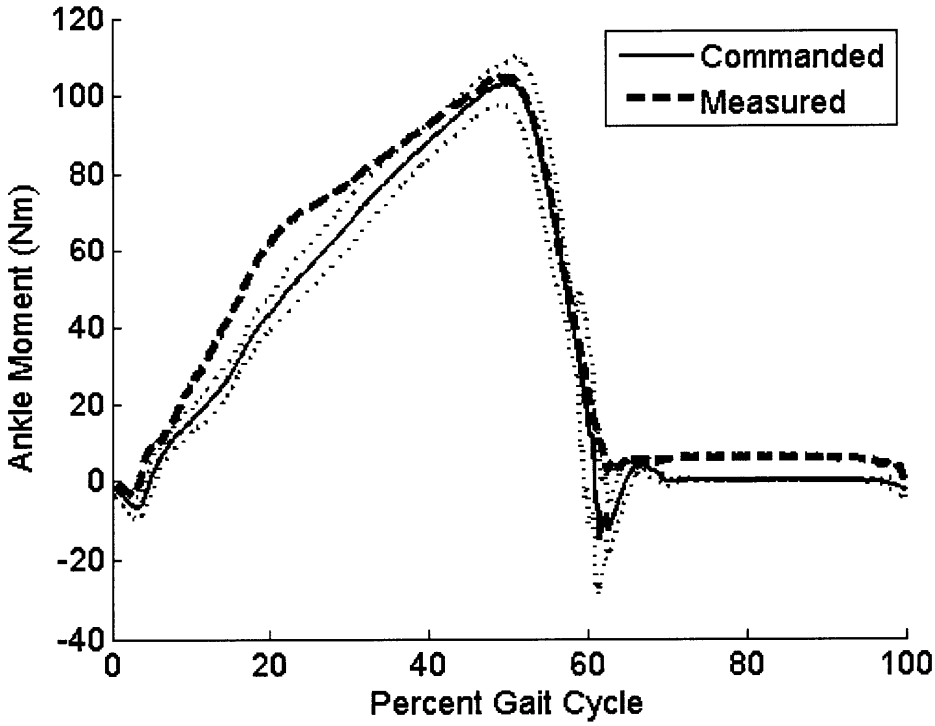

Figure 6-3: Torque-tracking for ramp ascent

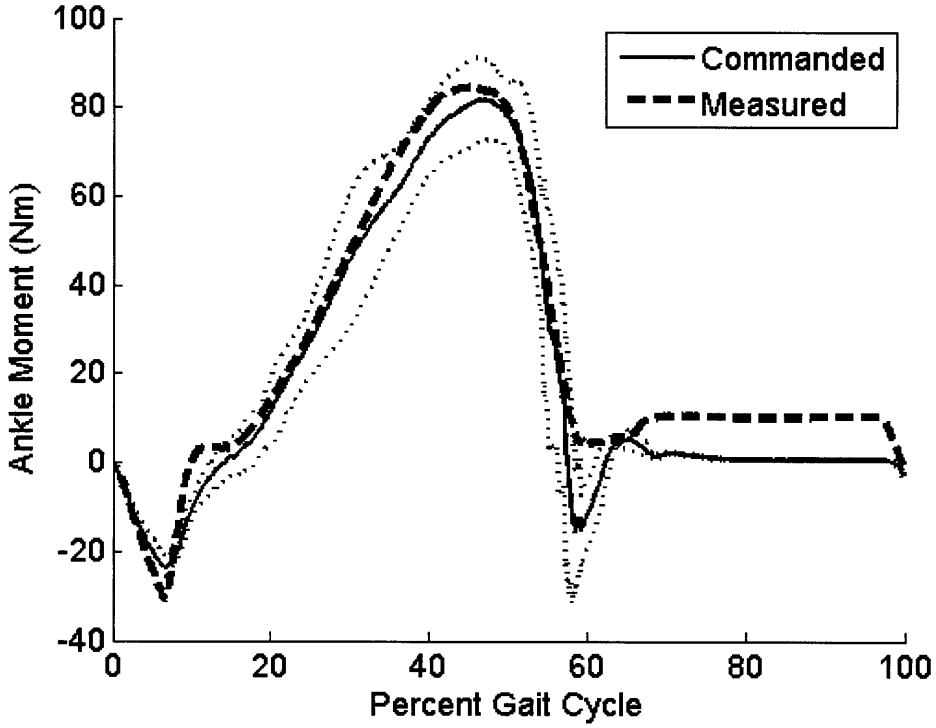

Figure 6-4: Torque-tracking for ramp descent

As expected, the measured torque for these trials closely followed the desired torque. However, during ramp ascent, (Figure 6-3) a large torque error was observed during CD (around 20% GC). This error is due to the fact that the commanded torque dropped below the parallel spring torque. Since cancellation of the parallel spring was not implemented, the ankle torque could not drop below the spring torque, and a tracking error occurred.

During the beginning of the swing phase, the apparent torque tracking error is likely caused by sensing inaccuracies of the series spring strain gauge at the low torque values and rapid motion associated with the onset of the swing phase. The offset seen during the rest of the swing phase can be attributed to a slight initial offset in the strain gauge measurement and friction in the drivetrain forcing a slightly positive ankle angle until heel-strike.

Also, during CP and beginning of CD, the ES state, not LS, was enabled. The force controller was therefore disabled during this section of the gait cycle, as mentioned in Chapter 5, leading to some tracking errors early in the stance phase.

Also of note, there existed a high-frequency torque ripple in the commanded prosthesis torque which cannot be seen in the averaged data shown. This is due to the fact that the output of the Hall-effect sensor is not smooth (as shown in Figure 4-8). The sensor ripple propagated through the neuromuscular model to produce an oscillatory component in the torque command. This effect, however, was not expected to change the results of the experiments.

6.3.2. Motor Saturation Verification

Since, according to Section 4.5, the motor was expected to saturate under the normal level-ground walking conditions, the motor behavior was analyzed for the moderate speed level-ground walking trials, as shown in Figure 6-5. The motor torque limit associated with the software-enforced current-limit of 25 Amps is also shown. The motor torque was estimated from the motor current and torque-constant. To estimate the hypothetical situation without the series spring, the motor velocity, ω, was estimated using the ankle velocity as computed from the Hall-effect sensor, $\dot{\theta}$, and the transmission ratio, R (using $\omega = R\dot{\theta}$).

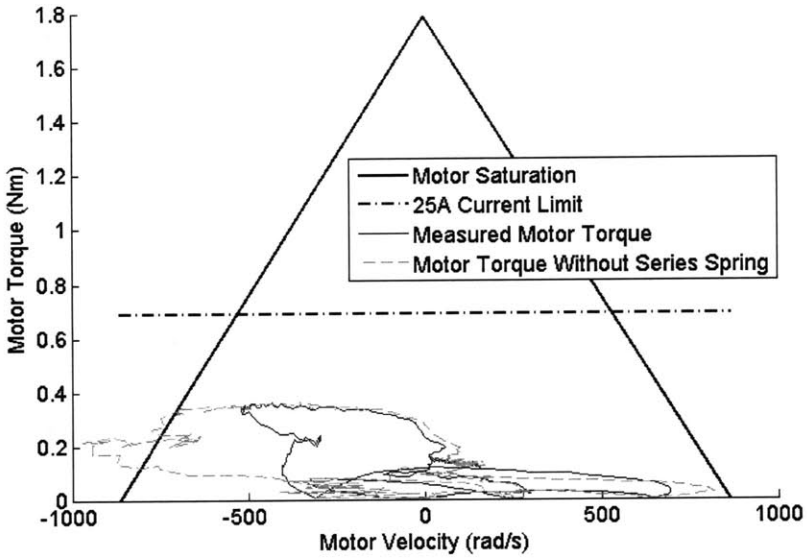

Figure 6-5: Average motor behavior during moderate-speed level-ground walking trials, and hypothetical situation without series spring

It is clear from the figure that the motor, on average, did not saturate during these trials. The individual trials were also checked separately to verify that motor saturation did not occur. It is important to note, however, that if the motor had been directly connected to the ankle joint through a transmission without the series spring, motor saturation would have occurred given the same torque-angle profile. The lack of saturation observed is therefore attributed to the ability of the series spring to quickly release stored energy [12]. This ability of the series spring to provide large amounts of instantaneous power is one of the primary reasons for using a series-elastic actuator [12].

6.3.3. Comparison to Biologic Data

In this section, the clinical trial results are compared to the torque and torque-angle profiles of the biologic data from Section 3.4.2.

6.3.3.1. Level-Ground Walking

The averaged ankle torque profiles of the level-ground walking trials are shown in Figure 6-6 and Figure 6-7 .

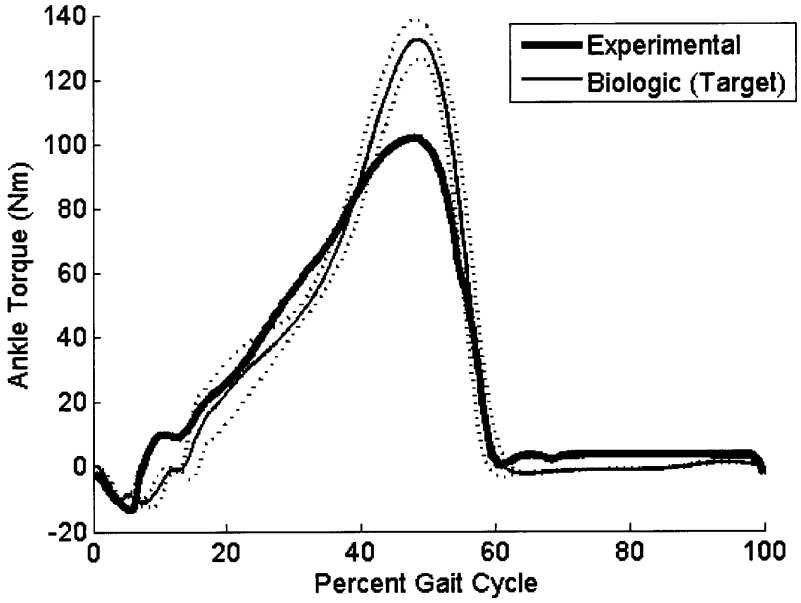

Figure 6-6: Ankle torque trajectory (moderate speed)

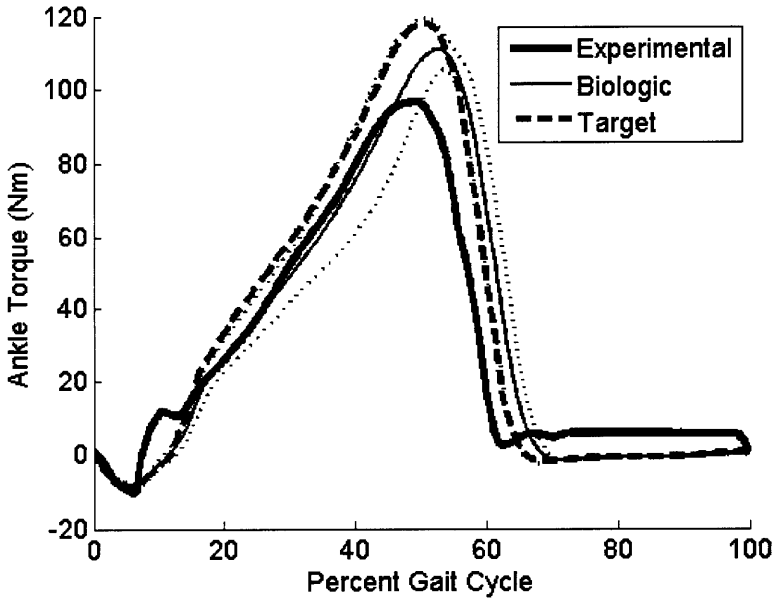

Figure 6-7: Ankle torque trajectory (slow speed)

The ankle angle, used as input to the neuromuscular model, is also shown for the two walking speeds in Figure 6-8 and Figure 6-9.

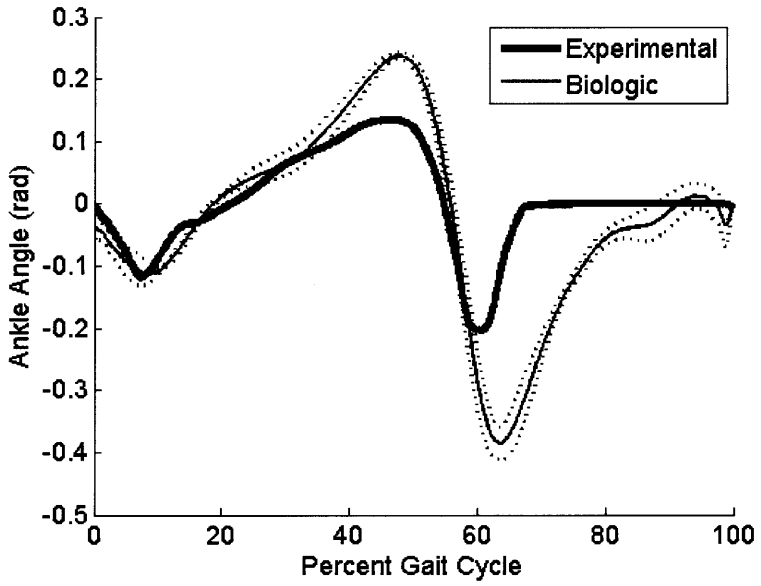

Figure 6-8: Ankle angle trajectory (moderate speed)

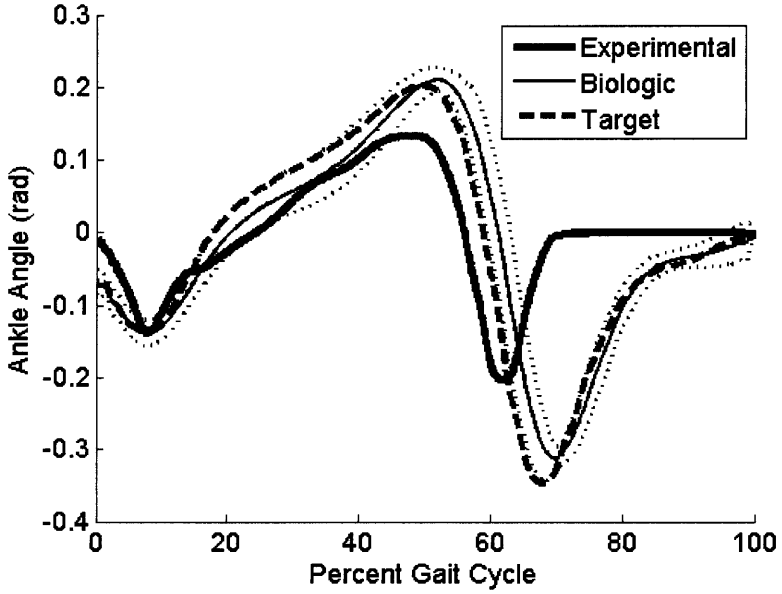

Figure 6-9: Ankle angle trajectory (slow speed)

The reflex architecture describes a relationship from ankle angle trajectory to ankle torque. It is therefore important to also analyze the behavior of the system in the torque-angle plane. Figure 6-10 and Figure 6-11 show the level-ground walking results in this form, again, compared against the biological data from which the muscle model was optimized. The markers defined in Figure 2-3 are shown for reference. The discrepancy

near the end of PP (towards the left side of the figures) between the measured and biologic torques is due to the angle threshold in LS described in Section 3.1.

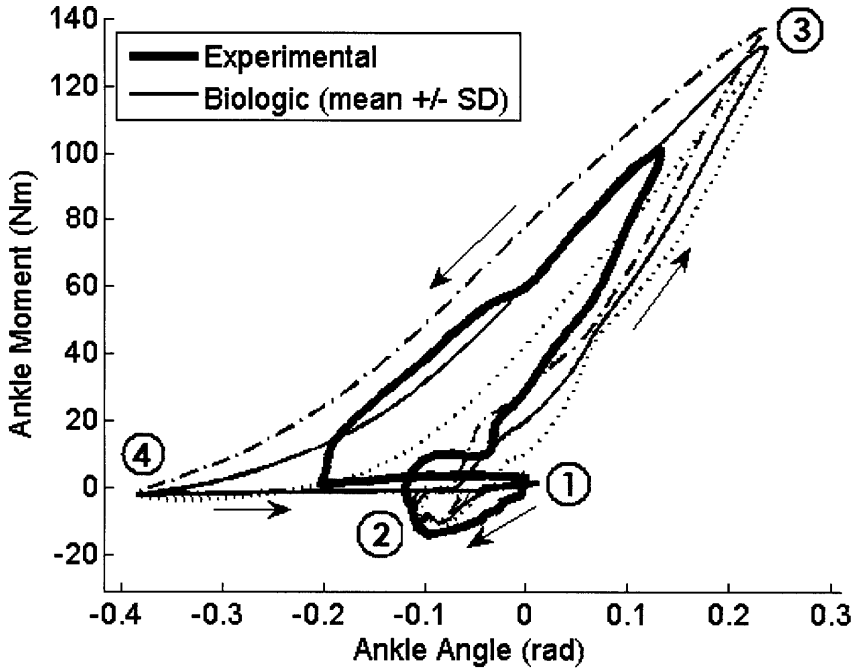

Figure 6-10: Torque vs. angle (moderate speed). The gait cycle is labeled at the same transition points as those described in Chapter 2: 1 is heel-strike, 2 is foot-flat, 3 is maximum dorsiflexion, and 4 is toe-off.)

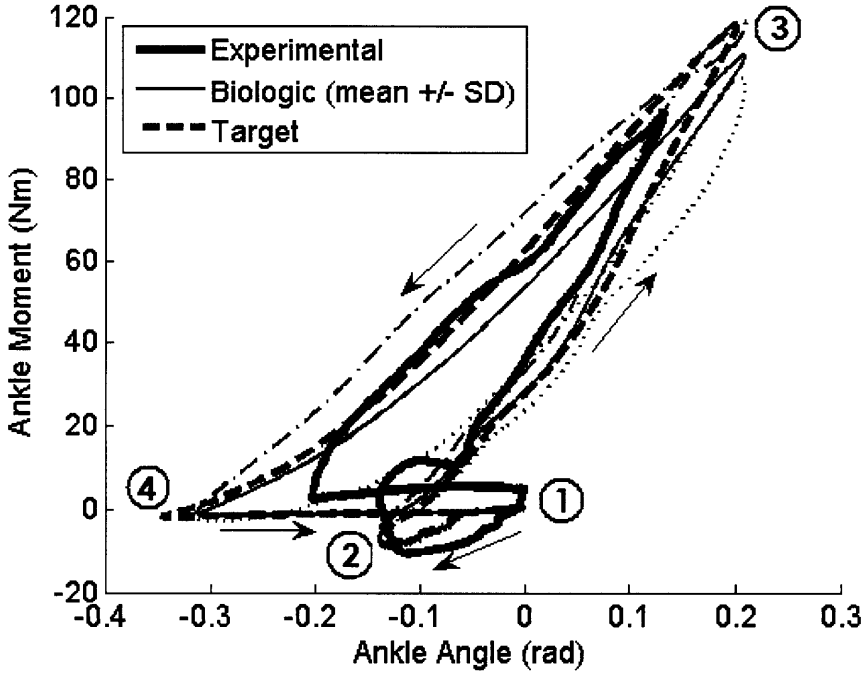

Figure 6-11: Torque vs. angle (slow speed)

6.3.3.2. Ramp Ascent and Descent

The corresponding torque-angle relationships can be seen for the ramp-walking trials. Once again, the angle threshold in LS prevents plantar flexion past 0.192 rad (11 deg). In addition, the Hall-effect sensor saturated near the beginning of CD in the ramp descent trials, as seen in Figure 6-13.

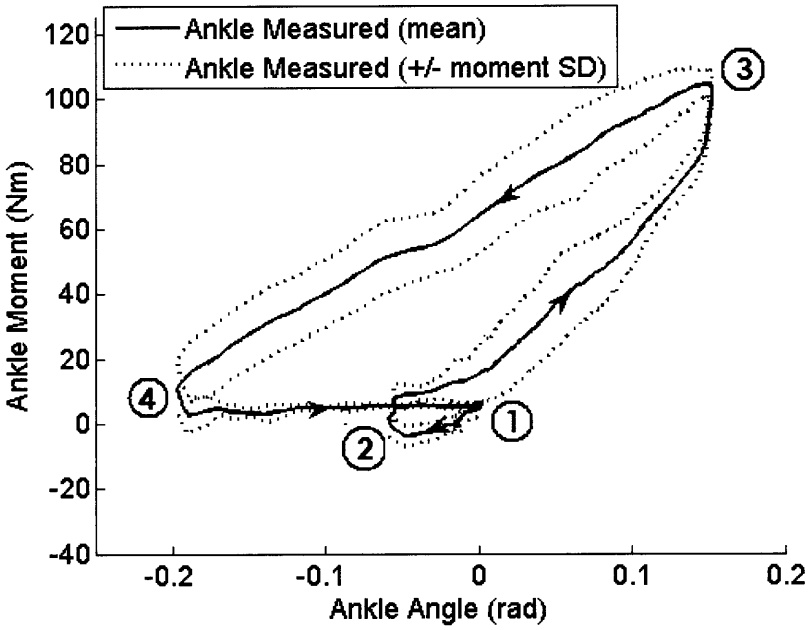

Figure 6-12: Torque vs. angle for ramp ascent

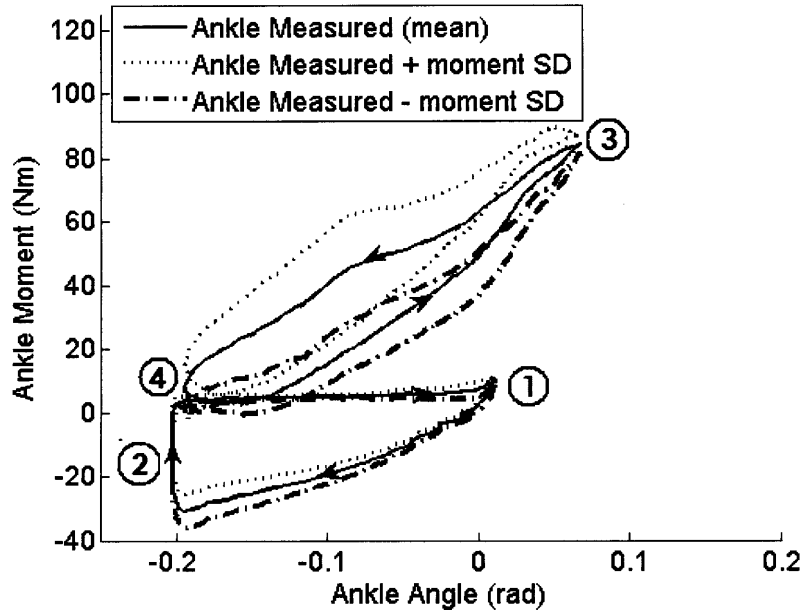

Figure 6-13: Torque vs. angle for ramp descent

6.3.4. Comparison Across Walking Conditions

To evaluate the hypothesis that positive net work changes across walking inclines, the torque-angle plots for each of the four walking conditions were plotted in Figure 6-14. In addition, a net-work calculation was performed for the stance phase of the individual gait cycles for all walking conditions, and an average net work value was then computed for each walking condition. The positive net work for the stance phase is summarized in Table 6-1.

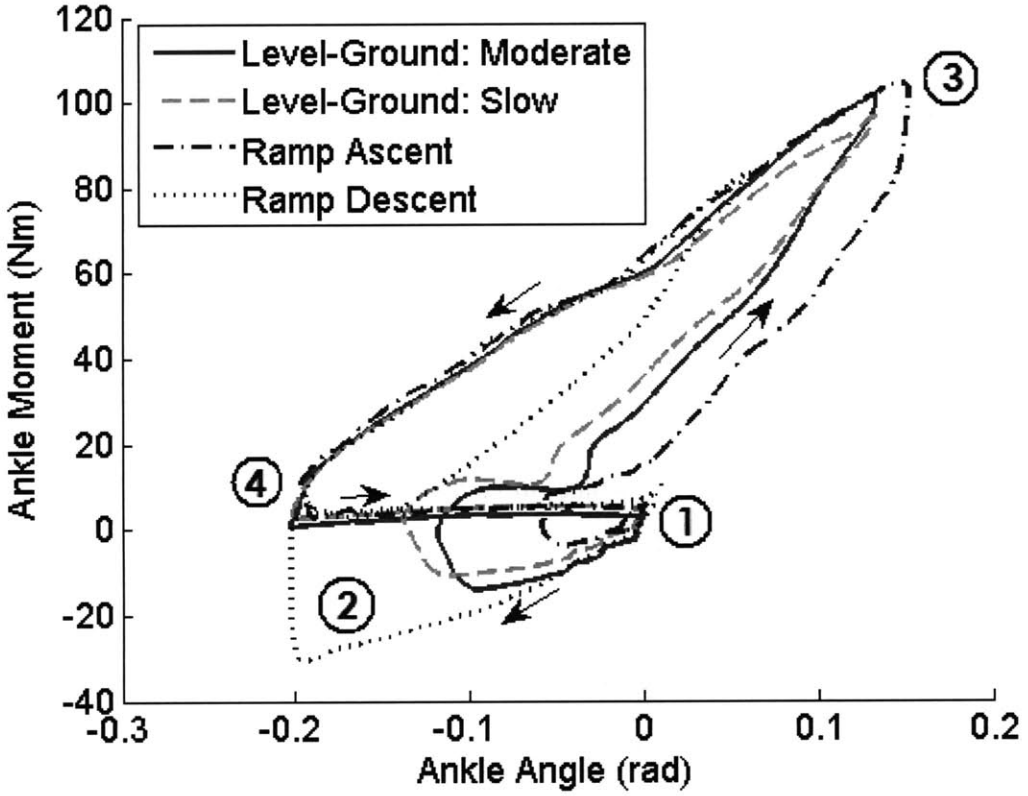

Figure 6-14: Torque vs. angle across walking conditions

Table 6-1: Prosthesis positive net work across walking conditions

Walking Condition (Parameter Set)	Positive Net Work (J)
Level-Ground (Moderate)	7.0 ± 0.5
Level-Ground (Slow)	5.4 ± 0.5
Ramp Ascent (Slow)	12.5 ± 0.6
Ramp Descent (Slow)	0.1 ± 1.7

6.3.5. Biologic Comparison for Ramp Gait

To provide a comparison between the clinical tests and biologic walking data, the net work from the ankle joint was calculated for averaged biologic walking trials of 11 healthy male subjects at self-selected speeds [10]. Analyses were performed on the following data from [10]: level-ground walking, ramp ascent, and ramp descent on a 10-degree incline. The resulting values of ankle net work are listed in Table 6-2

.

Table 6-2: Literature values for net work of the human ankle across walking conditions

Walking Condition	Positive Net Work (J)
Level-Ground	1.29
Ramp Ascent	24.9
Ramp Descent	-28.4

6.4. Discussion

6.4.1. Comparison to Biologic Torque

Focusing on the ankle stiffness (or slope in the torque-angle plane) early in the stance phase, it is clear that the prosthesis has the ability to exhibit the impedance change characteristic of the biological ankle, as discussed in Chapter 2, from CP to CD. This impedance modulation and associated energy storage is one indication that the behavior of the neuromuscular model is somewhat consistent with a biological ankle response. It is important to note that this behavior is not specified during the gait, but is emergent of the biologically-based structure of the neuromuscular model.

It is clear in Figure 6-6 and Figure 6-7 that the prosthesis produced peak torques considerably less than those of the biological ankle during the clinical trials. However, as Figure 6-8 and Figure 6-9 indicate, the prosthesis also failed to achieve the angle range of the biological ankle. The dependence of the model torque output on ankle angle implies that when the test subject selected an ankle angle trajectory that deviated from the biological ankle angle trajectory, a corresponding deviation in ankle torque was produced. This discrepancy in ankle angle trajectory was, in turn, due to a number of factors that changed the subject's response to a given ankle torque. These factors may include, but are not limited to: muscle atrophy and/or hypertrophy in the clinical test subject's leg muscles because of the amputations, differences in body mass, limb lengths, or flexibility between the clinical test subject and the subject with intact limbs. The existence of the amputation on the contralateral leg of the clinical test subject may also be a factor. Further tests are needed to narrow down the possible cause or causes of the angle trajectory discrepancy. Also, the angle threshold described in Section 3.1 limited the plantar flexion angle toward the end of PP. This angle limit further contributed to deviations in ankle angle from the biological trajectory. Nevertheless, the general

agreement in behavior between the biological ankle and the prosthesis indicates that this neuromuscular model can qualitatively represent the behavior of the human plantar flexor muscles during normal walking.

6.4.2. Positive Net Work Variation

The variation of stance-phase positive net work across walking conditions indicates a terrain-adaptive behavior that is emergent of the neuromuscular model. Referring to Table 6-1 and Table 6-2, the increased ankle net work during ramp ascent, and decreased ankle net work during ramp descent, compared to that of level-ground walking, is consistent with the trend seen in biology. This terrain adaptation is a consequence of the structure of the muscle model. The combination of muscle fiber length, fiber velocity, and time-history dependences enable the model to produce a variety of torque-angle curves based on the ankle state and state history. The difference in overall net work values between the clinical trials and the literature may be attributed to a difference in average walking speed between the literature and this clinical study, as well as the factors discussed in Section 6.4.1. The ability of the neuromuscular model to produce these biologic-like changes in behavior is further evidence that the model embodies the important characteristics of the human plantar flexor muscles.

As stated in Section 3.14.1, the prosthesis' ankle angle during PP was limited to 0.192 radians (11 degrees) of plantar flexion to avoid Hall sensor saturation. It is likely that the angle would have otherwise progressed past this artificial limit near the end of PP. In addition, the Hall sensor appears to have saturated during the transition from CP to CD during he ramp descent trials. From inspection of Figure 6-13, however, it is likely that the work-loop calculations over-estimated the net work for the ramp descent gait as a result of this saturation effect. Also, from Figure 6-10 and Figure 6-11, the contribution to total net work at the end of PP is relatively minor, and, from Figure 6-14, appears to be fairly consistent across walking conditions. For these reasons, neither the sensor saturation nor soft angle limit affect the final qualitative trend in net work production across terrain.

6.4.3. Speed Variability

Finally, the qualitative agreement between the prosthesis and the biological ankle behavior for the two different walking speeds indicates that the neuromuscular framework used in this thesis is capable of producing biologically-realistic behavior over varying walking speeds. Since the model's parameter values were modified with walking speed, this ability cannot be considered an automatic adaptation, but the results indicate that the model is at least capable of being tuned for use at multiple speeds.

7. Conclusions and Future Work

7.1. Conclusions

This thesis explored the use of a neuromuscular model for controlling an ankle-foot prosthesis. It has been shown that this model, when controlling a prosthesis worn by an amputee, has the capability of producing the qualitative level-ground walking behavior of the human ankle at two different gait speeds. In addition, it was shown that this model-based control strategy can automatically adapt to changing terrain by modulating the amount of positive net work produced at the ankle during the stance phase. These results underscore the importance of neuromuscular model-based control schemes for providing human-like ankle functionality across speed and terrain variations.

7.2. Future Work

7.2.1. Full Muscle Control

The clinical results demonstrate the viability of a Hill-type muscle model with positive force feedback as applied to the amputee gait. However, the existence of the proportional-derivative based dorsiflexor is still somewhat of an artificial addition to the model, since it is a very simple approximation of the dorsiflexor muscles. Future evaluations of this neuromuscular model should include a full-muscle control system consisting of an effective dorsiflexor muscle with length feedback [5] in addition to the plantar flexor muscle that was tested in this thesis. The addition of this second effective muscle would allow a simple stance phase switch to replace the finite state machine, thereby approximating the biologic system more closely.

7.2.2. High Level Motor Commands

Further analysis could be carried out regarding the use of a single set of model parameters to control a prosthesis at various stride rates. However, the inherent stabilization of stride energy of the positive force feedback-driven muscle model demonstrated in [5], as well as initial gait tests with this prosthesis, suggest that a single set of model parameters cannot apply for multiple walking speeds. It is likely, rather, that a neuromuscular model with one fixed parameter set would attempt to force a convergence in walking stride energy and, hence, speed. In such a case, a higher-level real-time controller must be developed for modulating neuromuscular parameters to achieve the desired overall behavior. In all likelihood, only neural-feedback parameters

would be modified by this higher level control, since other parameters represent inherent muscle properties that, in general, do not change.

7.2.3. Multiarticular Control

The eventual goal for this work is to enable multiple prosthetic joints to work together with an underlying, biology-based, model similar to the one tested in this thesis. The first step towards achieving this goal is to incorporate multiple joint states, such as those of the ankle and knee, into the control of a single prosthesis. Next, the modeled behavior of effective multiarticular muscles may be applied to the prostheses corresponding to the joints on which these muscles act, thereby producing virtual muscle connections between multiple prosthetic joints. Entire prosthetic limbs could eventually be controlled in this manner using a full-limb musculoskeletal model.

Appendix A

The genetic algorithm optimizer in Matlab (as described in Chapter 3) required multiple optimizer settings to be specified. The settings used in this thesis are shown in the following table.

Table A-1: Matlab GAtool Optimizer settings

Population Size	20	**Migration Fraction**	0.2
Pop. Creation Function	Uniform	**Migration Interval**	20
Pop. Initial Range	0-1	**Initial Penalty**	10
Scaling Function	Rank	**Penalty Factor**	100
Selection	Stochastic Uniform	**Hybrid Function**	fminunc
Elite Count	2	**Generations**	100
Crossover Fraction	0.8	**Time Limit**	Infinite
Mutation Function	Gaussian	**Fitness Limit**	Infinite
Mutation Scale	1.0	**Stall Generations**	50
Mutation Shrink	1.0	**Stall Time Limit**	20
Crossover Function	Scattered	**Function Tolerance**	1e-6
Migration Direction	Forward	**Nonlinear Constraint Tolerance**	1e-6

Hall-Effect Sensor Cubic Fit:

The Hall-effect angle sensor, as described in Chapter 4, was calibrated using a cubic polynomial of the form:

$$\theta_{ank} = aN^3 + bN^2 + cN + d \tag{6.1}$$

where N is the output of the Hall-effect sensor measured in analog-to-digital converter counts. The values for parameters a, b c are listed in Table A-2. A value for d was not obtained, since the zero-point of the sensor was able to be reset, and it was assumed that this reset point would always occur at the (fixed) engagement point of the parallel spring.

Table A-2: Polynomial fit values for Hall-effect angle sensor calibration

a	-1.2953e-13
b	1.1790e-9
c	4.5717e-4

Appendix B

C Code Implementation

The C code for the force controller implementation (as mentioned in Section 5.3) is included below. The function takes in the measured actuator torque error in units of N·m and returns the control effort also in units of N·m.

```
float single_lead (float torque_error){
        // Control system dynamics are in the form:
        //        k(s+z)/(s+p)  where z=zero location, p=pole location, k=gain

        static float et1 = 0;     // previous torque error value
        static float et2 = 0;     // second-to-last torque error value
        static float ut1 = 0;     // previous commanded torque value
        static float ut2 = 0;     // second-to-last commanded torque value

        float fcontrol_torque = 0.0;

        // allow the location of the zero and pole to
        // be moved using two tunable params

        float N1 = (2. + TS*x);
        float N2 = (TS*x - 2.);
        float D1 = (2. + TS*p);
        float D2 = (TS*p - 2.);

    // force controller difference equation:
        fcontrol_torque = k*(N1*torque_error + N2*et1 - D2*ut1)/D1;

        // update desired, commanded torque histories
        et2 = et1;
        et1 = torque_error;
        ut2 = ut1;
        ut1 = fcontrol_torque;

        return fcontrol_torque;
}
```

Bibliography

[1] S. K. Au, "Powered Ankle-Foot Prosthesis for the Improvement of Amputee Walking Economy", *Ph.D. Thesis*, Massachusetts Institute of Technology, 2007.

[2] S. K. Au, M. Berniker, H. Herr, "Powered ankle-foot prosthesis to assist level-ground and stair-descent gaits", *Neural Networks,* Vol. 21, Issue 4, pp 654-666, 2008.

[3] G. Franklin, J. Powell, M. Workman, *Digital Control of Dynamic Systems*, New Jersey: Addison Wesley Longman Inc; 1998.

[4] D. H. Gates, "Characterizing ankle function during stair ascent, descent, and level walking for ankle prosthesis and orthosis design", *Masters thesis*, Boston University, 2004.

[5] H. Geyer, A Seyfarth, and R. Blickhan, "Positive force feedback in bouncing gaits?", *Proceedings of Royal Society B-Biological Sciences, London,* Vol. 270, No. 1529, pp 2173-2183, 2003.

[6] A Hansen, D. S. Childress, S. C. Miff, S. A. Gard, K. P. Mesplay, "The human ankle during walking : implication for the design of biomimetic ankle prostheses", *Journal of Biomechanics,* Vol. 37, Issue 10, pp 1467-1474, 2004.

[7] H. Herr, M. Popovic, "Angular momentum in human walking", *The Journal of Experimental Biology*, Vol. 211, pp 487-481, 2008.

[8] H. Herr, A. Wilkenfeld, "User-adaptive control of a magnetorheological prosthetic knee", *Industrial Robot: An International Journal*, Vol. 30, Issue 1, pp 42-55, 2003.

[9] V. Hill, "The heat of shortening and the dynamic constants of muscle", *Proceedings of the Royal Society*, London, Ser. B 126, pp 136-195, 1938.

[10] A. S. McIntosh, K. T. Beatty, L. N. Dwan, and D. R. Vickers, "Gait dynamics on an inclined walkway", *Journal of Biomechanics*, Vol. 39, pp 2491-2502, 2006

[11] N. S. Nise, *Control Systems Engineering 3rd ed.* New York: John Wiley & Sons, Inc; 2000.

[12] D. Paluska, H. Herr, "Series Elasticity and Actuator Power Output", *Proceedings of the 2006 IEEE International Conference on Robotics and Automation,* Orlando, pp 1830-1833, 2006.

[13] J. Perry, *Gait Analysis: Normal and Pathological Function.* New Jersey: SLACK Inc.; 1992

[14] D. E. Rassier, B. R. MacIntosh, and W. Herzog, "Length dependence of active force production in skeletal muscle", *Journal of Applied Physiology,* Vol. 86, Issue 5, pp 1455-1457, 1999.

[15] D. Robinson, "Design and an analysis of series elasticity in closed-loop actuator force control", *Ph.D. Thesis*, Massachusetts Institute of Technology, 2000.

[16] K. S. Türker, "Electromyography: some methodological problems and issues", *Physical Therapy,* Vol. 73, No. 10, pp 698-710, 1993.

[17] www.maxon.com